Hydrogen combustion technologies for sustainable aviation

CAP 3118

Published by the Civil Aviation Authority 2025

Civil Aviation Authority
Aviation House
Beehive Ring Road
Crawley
West Sussex
RH6 0YR

In November 2022, the UK Government awarded the CAA a grant of £939,150 via the Regulators' Pioneer Fund to deliver the Hydrogen Challenge, which started in September 2023. The RPF is a grant-based fund to enable UK regulators and local authorities to help create a UK regulatory environment that encourages business innovation and investment. The current £12m round is being delivered by the DSIT.

This document has been prepared by Dr Zhaoxin Ren at the Department of Aerospace Engineering and the Zienkiewicz Institute for Modelling, Data and AI, University of Swansea, under the provisions of the CAA's contract 3551 "Academic research in support of the Hydrogen Challenge."

May 2025

Enquiries regarding the content of this publication should be addressed to: hydrogenchallenge@caa.co.uk

The latest version of this document is available in electronic format at: www.caa.co.uk/CAP3118

Contents

Abstract

This final report summarises the results and findings from the research project on "Hydrogen Combustion Technologies for Sustainable Aviation." Considering the typical missions of an aircraft using a CFM-56 turbine engine—including take-off, climb, cruise, and landing, as well as off-design scenarios—the report presents the numerical simulation tests of transient flow and combustion characteristics of direct injection of cryogenic hydrogen (80 K) in the combustion chamber. The flame dynamics and stability, lift-off position as a jet flame and temperature distribution are investigated. It outlines the development of operational guidelines for safe hydrogen utilisation in gas turbine engines and offers preliminary insights for engine design optimised for hydrogen fuel.

Chapter 1
Introduction

Hydrogen is a promising fuel for achieving net-zero carbon emissions in aviation. Unlike conventional jet fuel, hydrogen combustion produces no CO_2 emissions, making it a potential alternative for sustainable aviation. However, transitioning to hydrogen-powered aircraft requires extensive research into the combustion characteristics, stability, and safety implications of hydrogen in gas turbine engines considering different flight scenarios.

This study focuses on the transient combustion behaviour of cryogenic hydrogen (80 K) in a CFM56-type engine under various flight conditions. The key objectives are:

- To analyse hydrogen jet flame dynamics, including flame stability, lift-off distance, and flame structure.
- To assess the influence of air inlet conditions (speed, pressure, and temperature) on combustion performance.
- To develop operational maps for the safe and efficient use of hydrogen in gas turbine engines.

Underlying assumptions and justifications

Using hydrogen at cryogenic temperature (80 K)

Storing hydrogen in its liquid state (LH_2) is a key target for future aviation due to its high energy density, making it an economically favourable option for hydrogen storage. However, using cryogenic gaseous hydrogen ($CryoGH_2$) for combustion offers several advantages over direct LH_2 injection:

- Prevention of flash boiling & pressure fluctuations. If LH_2 were injected directly into the combustor, it could flash-boil due to the sudden temperature increase, causing strong pressure fluctuations and potential combustion instability. By evaporating LH_2 into ($CryoGH_2$) at 80 K before injection, phase change effects are eliminated, ensuring stable fuel delivery.
- Effective cooling of engine components. As LH_2 evaporates into $CryoGH_2$, it absorbs heat from surrounding engine components, providing effective cooling to engine components, reducing material stress and enhancing durability.

- Optimised expansion ratio for fuel transport. The expansion ratio of LH_2 (20 K) to $CryoGH_2$ (80 K) under the same pressure of 5 bar is approximately 16. In contrast, if hydrogen were used at ambient temperature (300 K), the expansion ratio would increase to ~800, creating significant challenges for fuel transport and injection system design. Using $CryoGH_2$ at 80 K achieves a balance between high density and manageable expansion, making it suitable for gas turbine applications.
- Avoiding icing of air components: 80 K is close to the boiling point of liquid nitrogen (77 K), a commonly used cooling material in cryogenic hydrogen storage systems. Injecting $CryoGH_2$ at 80 K into the combustor helps prevent the formation of ice on air components such as nitrogen, ensuring reliable operation.

Therefore, using hydrogen at 80 K provides an optimal balance between storage efficiency, combustion stability, cooling benefits, and system safety, making it a practical choice for hydrogen-powered aviation gas turbines.

Air inflow speeds at the combustion chamber inlet

The airspeed at the compressor outlet typically ranges from 100 m/s to 150 m/s, requiring a diffuser to decelerate the flow before it enters the combustion chamber to ensure stable combustion. However, excessive deceleration leads to energy losses due to non-ideal compression effects and wall friction losses.

To balance flame stability and energy efficiency, the airflow speed after the diffuser must be carefully chosen. For conventional kerosene-fuelled combustors, the airspeed is typically around 5 m/s. However, hydrogen flames propagate at a higher speed than kerosene flames, necessitating a higher airflow speed to maintain stable combustion.

Therefore, in this study, 10 m/s and 20 m/s were selected for a comparative investigation of hydrogen combustion behaviour.

Pressure and temperature at the combustion chamber inlet

The air pressure and temperature conditions at the combustion chamber inlet were determined based on:

- Flight envelope data: The values were extracted from CFM56 engine performance data and scaled to represent realistic mission profiles.
- Altitude and atmospheric conditions: Using the International Standard Atmosphere (ISA) model, the following static pressure and temperature values were applied:

Table 1 Combustion chamber inlet conditions for each flight phase.

FIIGHT PHASE	STATIC PRESSURE (bar)	STATIC TEMPRERAT URE (K)
TAKE-OFF	8.0	700
CLIMB	6.0	600
CRUISE	2.0	400
DESCENT/LANDING	3.0	300
OFF-DESIGN: HOT & HIGH	7.0	800
OFF-DESIGN: FLAME-OUT (25,000 FT)	0.44 – 0.57	250 - 280
OFF-DESIGN: RELIGHT (37,000FT)	0.39	280

The air pressure and temperature inside the combustion chamber vary depending on the inlet conditions and the combustion process:

- Higher pressure and temperature at take-off and climb improve flame stability, ensuring effective ignition and sustained combustion.
- Lower pressure and temperature at cruise and descent reduce the risk of thermal NOx formation while maintaining stable combustion.
- Flame-out scenarios at high altitudes (e.g., 25,000 ft and 37,000 ft) involve extremely low air pressure, which affects ignition reliability and requires extended ignition times.

The numerical simulations account for these variations by solving the compressible Navier-Stokes equations with a detailed chemical reaction mechanism, which will be detailed in the following sections.

Digital twin and mapping to the experimental test rig

To ensure accurate numerical simulations, the physical combustion test rig at Loughborough University was used to model the combustion chamber. The geometry of the Loughborough Rolls-Royce UTC test facility was mapped to the digital twin simulation model, considering:

- Combustor dimensions: The test rig's single-jet configuration with the same dimension was used to isolate combustion effects without interference from multi-jet interactions.
- Injection and mixing: The fuel injection characteristics and air mixing patterns observed in the experimental setup were replicated in the computational domain to match physical test conditions.

This approach ensures that the numerical model accurately represents real-world combustion physics, while also enabling parametric studies on hydrogen combustion under various operating conditions.

Ignition model from engine running conditions

In the Loughborough test rig, ignition is initiated via a spark plug, similar to how aerospace gas turbines are ignited at the start of a flight. However, in the numerical simulations, individual ignition events are required for each flight phase separately.

- The simulations for each flight stage were conducted independently, simulating separate ignition for each phase.
- Additionally, a one-time ignition model was considered for transitions between different flight phases, eliminating the need for repeated ignition across the mission.
- A hot spot ignition model was applied with an ignition duration of several milliseconds, comparable to ignition times in actual gas turbine engines.

Chapter 2

Mathematical model and methodology

The study employed numerical experiments using the high-fidelity HiSMART simulation solver [1]. HiSMART solves the Navier-Stokes equations together with the mass fraction equations of chemical species for the compressible, multi-component and reactive flows, described as follows,

$$\frac{\partial}{\partial t}(\rho)+\frac{\partial}{\partial x_j}\left(\rho u_j\right)=0 \tag{1}$$

$$\frac{\partial}{\partial t}\left(\rho u_i\right)+\frac{\partial}{\partial x_j}\left(\rho u_i u_j+P\delta_{ij}-\tau_{ij}\right)=0 \tag{2}$$

$$\frac{\partial}{\partial t}\left(\rho e_{\mathrm{t}}\right)+\frac{\partial}{\partial x_j}\left(\left(\rho e_{\mathrm{t}}+P\right)u_j-u_i\tau_{ij}-q_j\right)=0 \tag{3}$$

$$\frac{\partial}{\partial t}\left(\rho Y_k\right)+\frac{\partial}{\partial x_j}\left(\rho Y_k u_j\right)+\frac{\partial}{\partial x_j}\left(\rho Y_k\left(V_{k,j}+V_j^{\mathrm{c}}\right)\right)=S_{\mathrm{combustion},k} \tag{4}$$

In the above equations, the density, velocity vector, static pressure, and total energy of the reactive mixture are represented by ρ, u_i, P, and e_{t}, respectively. e_{t} is kinetic energy plus internal (containing chemical) energy, which is defined as,

$$e_{\mathrm{t}}=\sum_{k=1}^{N_S}Y_k\left(\int_{T_{\mathrm{ref}}}^{T}c_{p,k}\mathrm{d}T+h_{f,k}^{0}\right)-\frac{P}{\rho}+\frac{u_iu_i}{2} \tag{5}$$

where $c_{p,k}$ is the specific heat capacity at constant pressure and $h0\ f,k$ is the specific chemical formation enthalpy at the reference temperature, T_{ref}. Furthermore, τ_{ij} is the Newtonian viscous stress tensor, and μ is the viscosity. Y_k is the mass fraction of the k^{th} species. $Vc\ j$ is the correction velocity. The kinetic theory for a gaseous mixture is used to compute the transport and thermodynamic properties of the gaseous mixture [2]. The Lennard-Jones potential is used to calculate the intermolecular forces. The heat conductivity of each species is calculated by using the modified Eucken model. The dynamic viscosity and the binary diffusion coefficient are computed according to the Chapman-Enskog theory.

$$\mu_k=\frac{26.69\sqrt{W_kT}}{\sigma_k^2\Omega_{v,k}} \tag{6}$$

$$\frac{\lambda_kW_k}{\mu_kC_{v,k}}=1.32+\frac{1.77}{\left(C_{p.k}/R\right)-1} \tag{7}$$

$$D_{AB}=\frac{0.00266T^{3/2}}{PW_{AB}^{1/2}\sigma_{AB}^2\Omega_D} \tag{8}$$

Here, σ_k is the hard-sphere diameter of the k^{th} species. D_{AB} is the diffusion coefficient for the binary gas A and B, W_{AB} is the combined molecular weights of A and B. σ_{AB} is the characteristic length of the intermolecular force law, and Ω_D is the collision integral for diffusion. The semi-empirical expressions proposed by Wake and Wassiljewa [2] are used to calculate the dynamic viscosity, μ, and heat conductivity, λ, of the gaseous mixture.

$$\mu_m = \sum_{i=1}^{n} \frac{X_i \mu_i}{\sum_{j=1}^{n} X_j \varphi_{ij}} \tag{9}$$

where X_i and X_j are the mole fraction of the components i and j. The function is as follows,

$$\varphi_{ij} = \frac{\left(1 + \left(\mu_i / \mu_j\right)^{1/2} \left(W_j / W_i\right)^{1/4}\right)^2}{\left(8\left(1 + W_i / W_j\right)\right)^{1/2}} \tag{10}$$

$$\lambda = \sum_{i=1}^{n} \frac{X_i \lambda_i}{\sum_{j=1}^{n} X_j A_{ij}} \tag{11}$$

where the function A_{ij} is $A_{ij} = \frac{\left(1 + \left(\lambda_i / \lambda_j\right)^{1/2} \left(W_j / W_i\right)^{1/4}\right)^2}{\left(8\left(1 + W_i / W_j\right)\right)^{1/2}}$.

The Noble-Abel Stiffened (NASG) gas equation of state (EOS) [3] is used to close the governing equations. It can be used to model the liquid and gas in a framework. For a single component, the NASG EOS is expressed as,

$$P = \frac{\rho(\gamma - 1)e}{1 - b\rho} - \gamma P_\infty \tag{12}$$

Chapter 3
Validation

Validation of HiSMART for cryogenic hydrogen reactive flows has been performed in two areas: namely flow and combustion features.

Flow process validation

Before validating the predictive capability of cryogenic hydrogen flow, the accuracy of the hydrogen thermodynamic properties must first be assessed. The validation is conducted using benchmark data from NIST at cryogenic temperatures, comparing the predicted thermodynamic properties of cryogenic hydrogen from HiSMART, as shown in Fig. 1. The results show that the two curves closely overlap for 1 bar conditions and for 10 bar conditions above 70 K, confirming that HiSMART provides reliable predictions. This validation supports the accuracy of the current simulations using cryogenic hydrogen at 80 K.

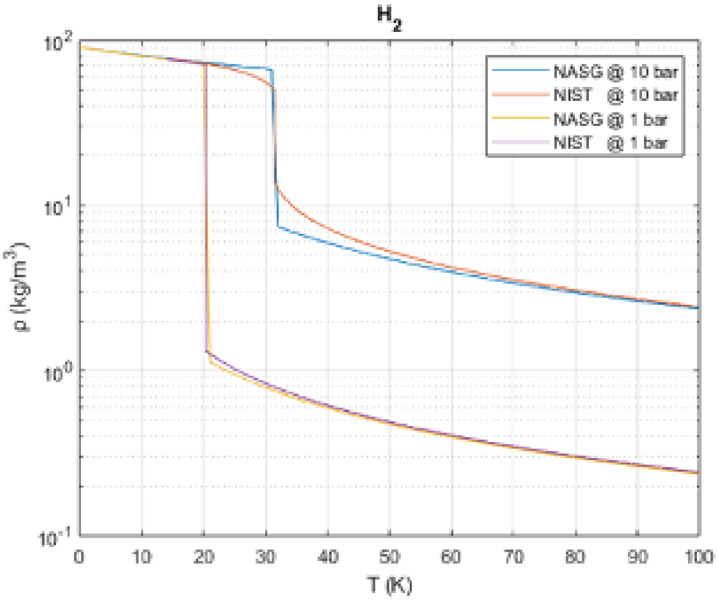

Figure 1 A graph showing hydrogen density comparison: HiSMART with NASG vs NIST database.

A cryogenic hydrogen jet (80 K) flow is then simulated [8]. The predicted axial hydrogen concentration statistics of the unignited jet are compared with the measurements of Friedrich et al. [9] in Fig. 2, in which X_{H2} is the axial centreline hydrogen mole fraction and z (m) represents the streamwise positions. The experiments measured hydrogen mole fractions at 0.5, 1.0 and 1.5 m along the centreline. Some small discrepancies exist between the predicted and measured concentrations. This is likely due to the small difference in the turbulence level at the inlet boundaries. In the numerical simulation, it was specified as 5% while the level of turbulence at nozzle exit in the experiment was not characterized. Nevertheless, the differences are very small, and the present solver is validated to simulate hydrogen dispersion. The predictions serve to inform the setup of the subsequent numerical simulations of the ignited jets.

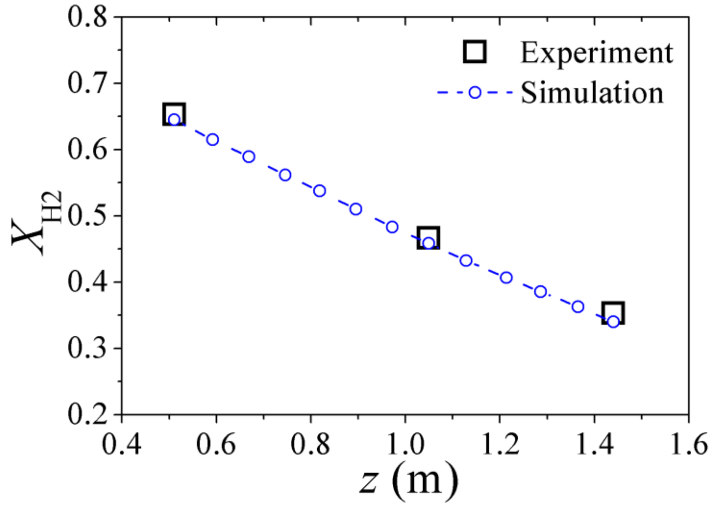

Figure 2 Comparisons of predicted and measured axial hydrogen concentration [8].

Another verification considers the fluid dynamics and checks the prediction ability of the current model for cryogenic hydrogen flow. Data from NASA's critical flow experiments of cryogenic hydrogen [10] is used to compare the results from the present numerical simulations, and the mass flow rates as shown in Fig. 3. The mass flow rates of the releasing cryogenic hydrogen with initial total pressures from around 10 bar to 60 bar were measured in the experiments, and it is found that the overall agreement between predicted and measured mass fluxes is reasonably good.

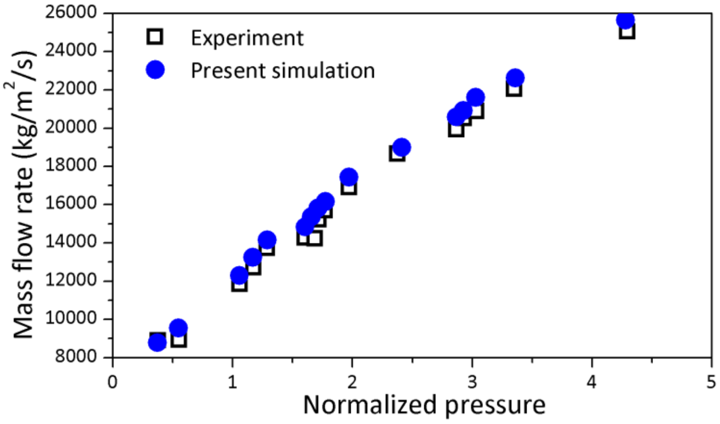

Figure 3 Comparison of NASA's cryogenic hydrogen release experiment data and present simulation results.

Combustion validation

Although the reaction mechanism used in the present simulation has been validated for a wide range of temperatures and pressures to describe the ignition delay times and flame speeds, it needs to be further validated by predicting the cell size of the detonation wave as it propagates in hydrogen-air mixtures at cryogenic temperatures using the current thermophysical model and detailed chemical mechanism. The detonation cell size is a measurement of the combustible mixture [11] and can be used to identify the heat release rate across the detonation wave. Compared to the cell size of the detonation wave across the reactive mixture at room temperature, the size at cryogenic temperatures is larger at fuel-lean conditions [11]. Fig. 4 shows the detonation cell size at different concentrations. The initial pressure for the calculation of detonation cell size is 50 atm. The cell size is measured along the direction perpendicular to the propagation direction of the detonation wave, and this corresponds to the vertical direction, consistent with the size measured in the experiments [11]. It is found that the cell size predicted by the present simulation is slightly larger than the size measured in the experiment. The current models can provide a reasonable cell size at different fuel concentrations.

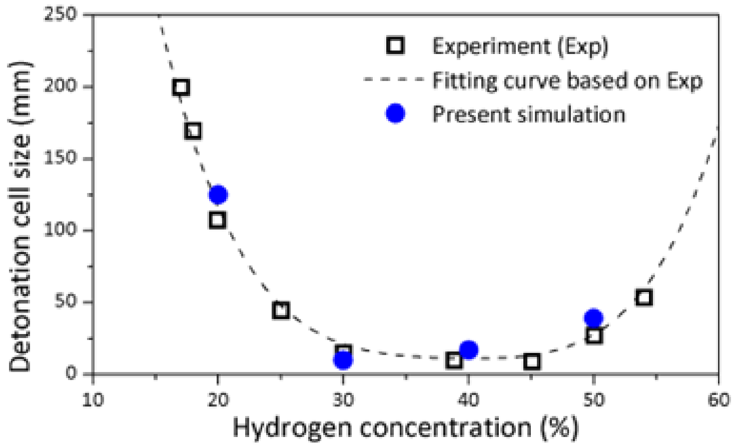

Figure 4 Detonation cell size of cryogenic hydrogen at different concentrations.

Chapter 4

Physical model and computation set-up

Micro-mix combustion was selected for hydrogen fuel due to its ability to achieve effective fuel injection, mixing, and non-premixed combustion properties, which helps mitigate flashback risks. The Loughborough University Rolls-Royce UTC combustion test rig served as the model framework [12], representing the fuel injection region (highlighted in the green box in Fig. 5) scaled from a gas turbine engine.

This study focuses on hydrogen jet combustion within the gas turbine combustion chamber. In real engines, fuel is typically injected perpendicular to the airflow using an impingement injection system, which enhances fuel-air mixing due to strong momentum exchange. However, this configuration also results in total pressure losses because of momentum offset in opposite directions.

Injection strategy and mixing performance:

- Total pressure represents the total energy of the airflow. Any pressure loss reduces usable energy, converting it into heat or turbulence, which negatively impacts the engine’s performance.
- Hydrogen gas has a much higher diffusion rate compared to kerosene vapour, allowing for better fuel-air mixing without requiring impingement injection.
- The Loughborough combustion rig employs a purely parallel injection pattern, which relies on shear mixing between hydrogen and airflow, rather than momentum exchange. This approach aims to enhance mixing efficiency without perpendicular injection, and reduce total pressure losses, thereby improving overall engine performance.

Single jet model vs. Full-scale engine combustion

- The numerical simulations focus on a single injection jet, rather than a multi-nozzle array.
- While this provides valuable insights into fundamental flame behaviour, it does not fully replicate the complexity of a full-scale gas turbine, where multiple nozzles interact, generating vortex structures and turbulent flame interactions.
- The present simulations isolate a single jet to study flow dynamics and composition changes without interference from surrounding flows, as depicted in Fig. 6.

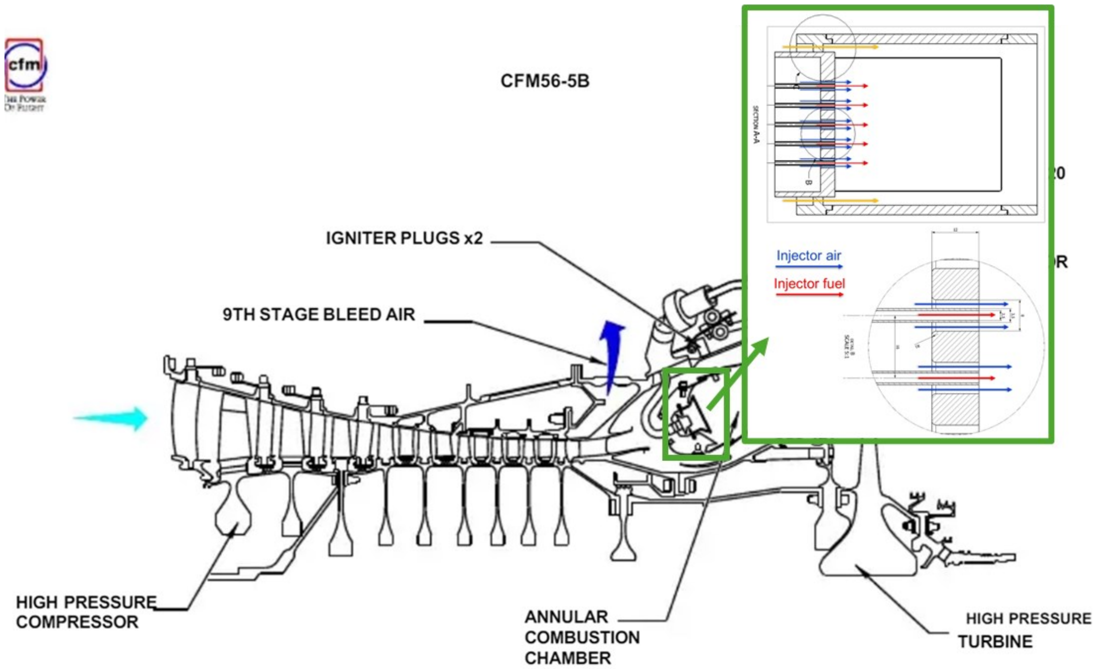

Figure 5 Geometry of the combustion test rig [12] in a gas turbine engine.

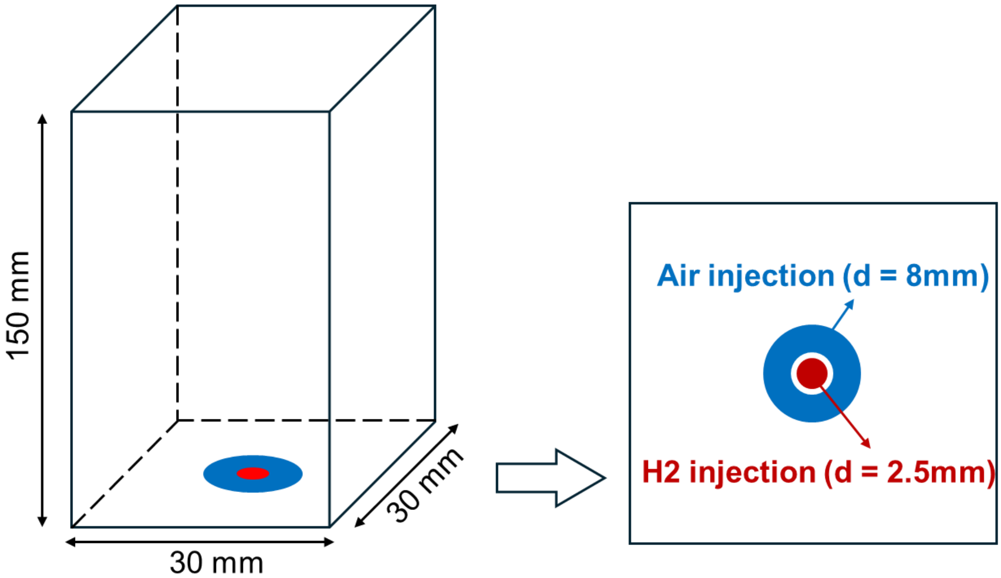

Figure 6 Physical model and computation domain.

For a typical CFM56 turbine engine operating during a flight mission, the combustion chamber inlet conditions were varied to simulate different flight stages. Cryogenic hydrogen (80 K) - the same temperature as liquid nitrogen, which is commonly used as a cooling material to maintain hydrogen storage temperatures [13] was used to ensure gaseous state compatibility.

Two air velocities (10 m/s and 20 m/s) were applied to represent low and high inflow conditions, respectively. Stoichiometric combustion (equivalence ratio of unity) was maintained by adjusting the hydrogen injection speed according to the air mass flow rate.

For simulation stability, the combustion chamber was initially filled with nitrogen, and ignition was initiated using a 2000 K spark model at a predefined position. The simulation cases are summarised in Table 2.

Table 2 Cryogenic hydrogen combustion test map.

H2 Combustion in Steady Flight Conditions	Air speed (m/s)
Take off (Air inlet: 8 bar, 700 K)	10
	20
Climb (Air Inlet: 6 bar, 600 K)	10
	20
Cruise (Air Inlet: 2 bar, 400 K)	10
	20
Desent/Landing (Air Inlet: 3 bar, 300K)	10
	20

H2 Combustion in Off-Design	Air speed (m/s)

Flight Scenarios	
Take-off under "hot and high" (Air Inlet: 7 bar, 800 K)	10 20
Flame out to 25,000 ft [5% max N2 shaft speed] (Air Inlet: 0.44 bar, 250 K)	10 20
Flame out to 25,000 ft [20% max N2 shaft speed] (Air Inlet: 0.57 bar, 280 K)	10 20
Relight at 37,000 ft [20% max N2 shaft speed] (Air Inlet: 0.39 bar, 280K)	10 20
Continuous Ignition during take-off stage (Air inlet: 8 bar, 700 K)	10 20

H2 Combustion During Flight State Transitions	Air speed (m/s)
From Take Off (Air Inlet: 8 bar, 700K) to Climb (Air Inlet: 6 bar, 600 K)	10 20
From Climb (Air Inlet: 6 bar, 600 K) to Cruise (Air Inlet: 2 bar, 400 K)	10 20
From Cruise (Air Inlet: 2 bar, 400 K) to Desent/Landing (Air Inlet: 3 bar, 300K)	10 20

Chapter 5

Results and discussion

Hydrogen combustion in steady flight conditions

Take-off stage

For an inflow air speed of 20 m/s, stable combustion was achieved following ignition at 28.0 ms. The spark (at 2000 K) initiates rapid flame development around the spark kernel, with the flame stabilising by 31.0 ms. The flame maintains self-sustaining properties even after spark deactivation at 36.0 ms, anchoring around x = 0.75 m. For an inflow air speed of 10 m/s, flame propagation was slower, and the lift-off distance was shorter, indicating reduced upstream propagation resistance.

High-speed air inflow (20m/s)

After fuel and airflow fill the chamber, ignition begins at 28.0 ms with a 2000 K spark. The flame rapidly develops around the spark kernel, stabilising by 31.0 ms with the spark's assistance, as shown in Fig. 7. Ignition persists for 8.0 ms, establishing stable combustion.

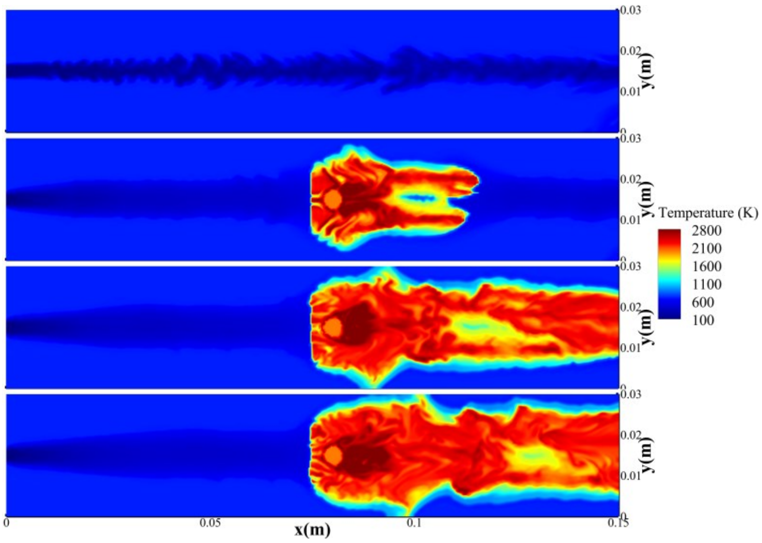

Figure 7 Flame's initial evolution of case 'Airspeed of 20 m/s for take-off stage'. Time from 28.0 ms to 31.0 ms (snapshots from up to bottom taken every 1.0 ms).

After the ignition is turned off at 36.0 ms, combustion continues stably without further spark heating, as shown in Fig. 8. The flame propagates slightly upstream and stabilises at x = 0.75 m.

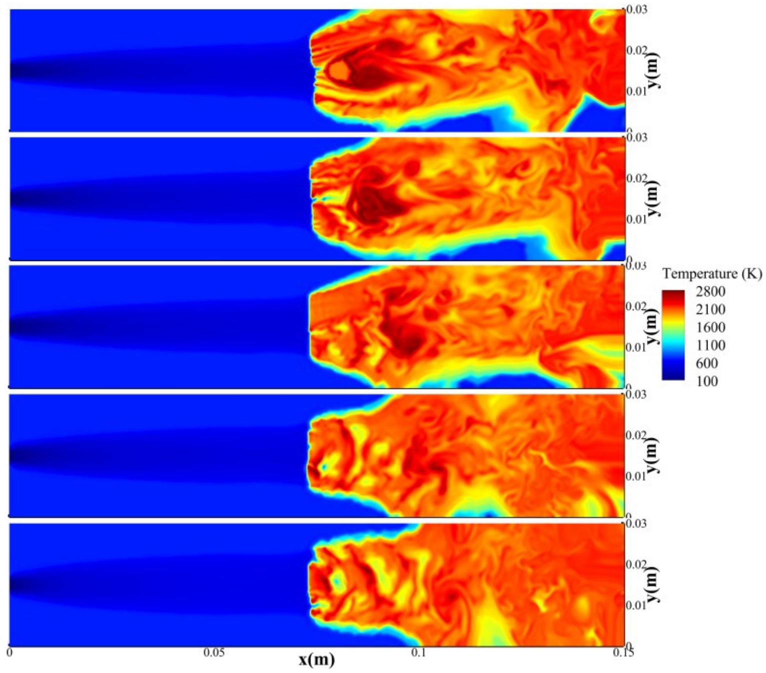

Figure 8 Flame's self-evolution of case 'Airspeed of 20 m/s for take-off stage' after spark deactivation. Time from 36.0 ms to 40.0 ms (snapshots from up to bottom taken every 1.0 ms).

Low-speed air inflow (10 m/s)

As airflow enters the combustion chamber at an inflow speed of 10 m/s, the flame propagates downstream more slowly after ignition, which occurs at 30.0 ms following the introduction of a spark. The ignition lasts for 8.0 ms, ending at 38.0 ms. This reduced speed of the incoming air limits the rate at which the flame travels downstream, as the lower flow speed carries the flame with it (Fig. 9).

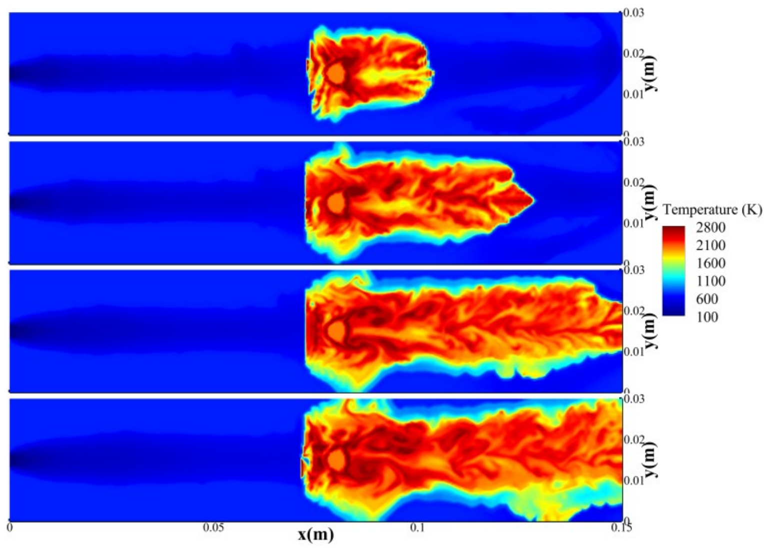

Figure 9 Flame's initial evolution of case 'Air speed of 10 m/s for take-off stage'. Time from 31.0 ms to 34.0 ms (snapshots from up to bottom taken every 1.0 ms).

Once the spark is turned off, the flame begins to propagate upstream. In this scenario, the flame moves at a speed that surpasses that observed with an inflow air speed of 20 m/s, as shown in Fig. 10. The lower speed (10 m/s) airflow provides less resistance against upstream flame propagation, resulting in a shorter lift distance from the injection nozzle where the flame is anchored, compared to the case with the higher inflow speed.

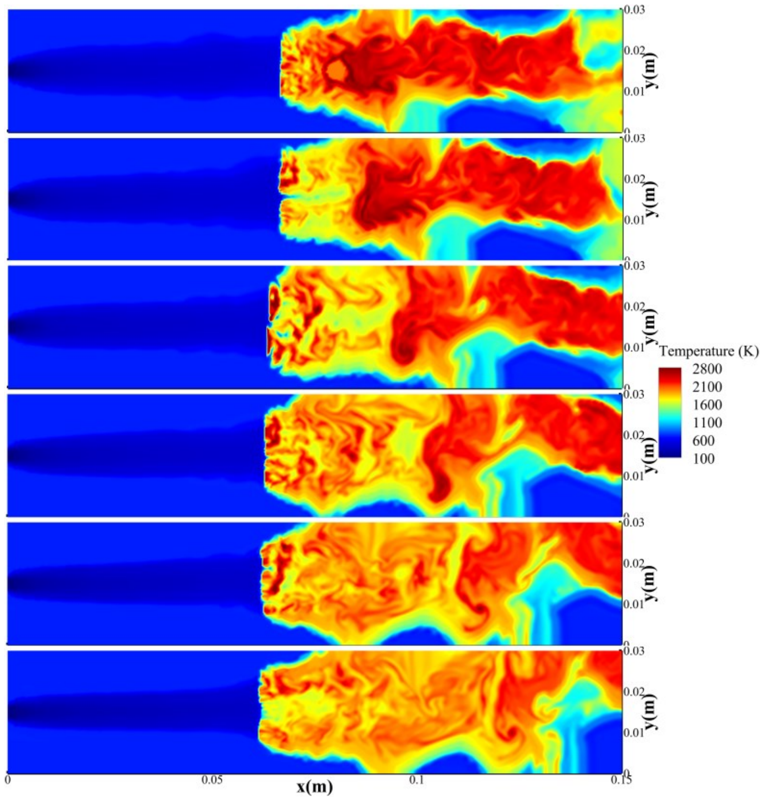

Figure 10 Flame's self-evolution of case 'Air speed of 10 m/s for take-off stage' after spark deactivation. Time from 38.0 ms to 48.0 ms (snapshots from up to bottom taken every 2.0 ms).

Climb stage

In this stage, with an inflow speed of 20 m/s, the flame expanded both upstream and downstream post-ignition, with multiple flame tips forming due to high incoming flow velocities. At 10 m/s, the flame propagation exhibited symmetrical behaviour and stabilised at x = 0.04 m, suggesting effective upstream anchoring.

High-speed air inflow (20 m/s)

With an inflow air speed of 20 m/s, the hydrogen and air mixture are injected into the chamber, and the spark is activated at 31.2 ms. Ignition occurs immediately at this time, lasting for 7.8 ms until 39.0 ms.

Fig. 11 illustrates the initial development of the hydrogen flame, displaying the instantaneous distributions of static temperatures. The mixture surrounding the spherical spark ignites almost instantly, owing to the low chemical activation energy of hydrogen, which allows ignition even at very low temperatures.

The flame then propagates in both upstream and downstream directions. However, due to the high speed of the incoming flow, the flame is unable to advance significantly upstream. In the downstream region, the flame rapidly spreads to fill the chamber.

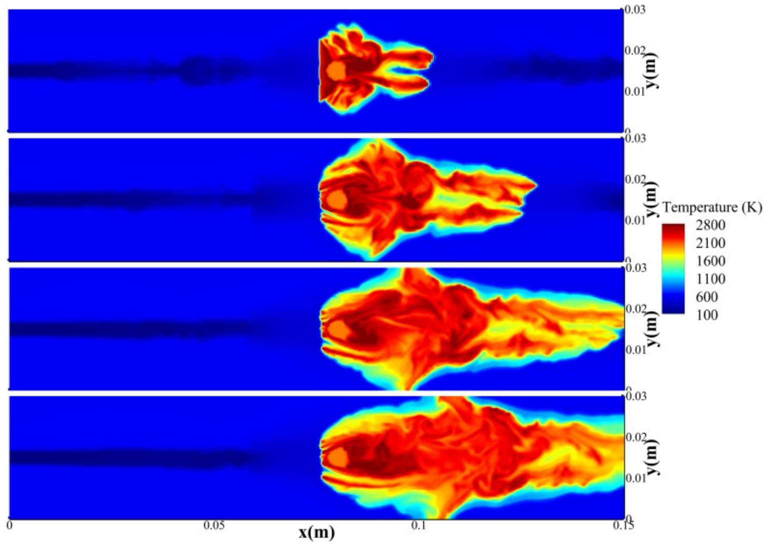

Figure 11 Flame's initial evolution of case 'Airspeed of 20 m/s for climb stage'. Time from 32.0 ms to 35.0 ms (snapshots from up to bottom taken every 1.0 ms).

The spark is turned off at 39.0 ms after the flame has been established in the combustion chamber. Fig. 12 illustrates the self-sustained propagation of the hydrogen flame. Following the cessation of the spark, the hydrogen flame propagates upstream and becomes anchored around the streamwise location of x = 0.075 m. Notably, this case exhibits multiple flame tips at the flame front, which distinguishes it from other observed cases.

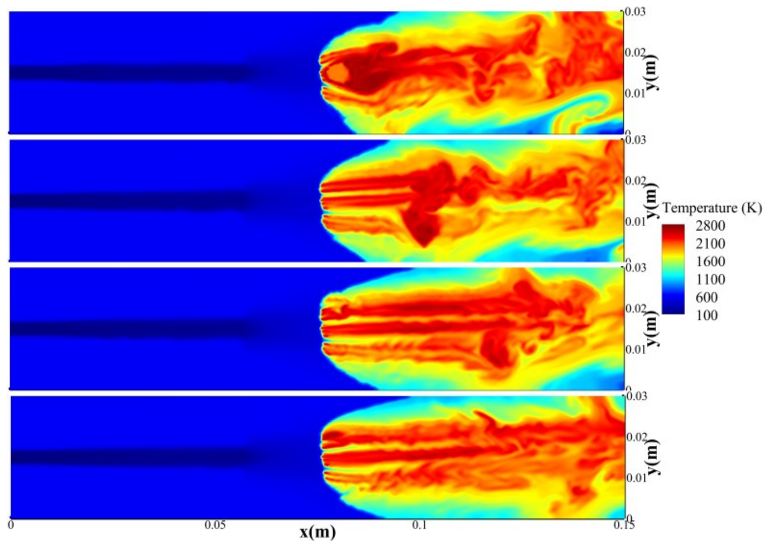

Figure 12 Flame's self-evolution of case 'Airspeed of 20 m/s for climb stage' after after spark deactivation. Time from 39.0 ms to 45.0 ms (snapshots from up to bottom taken every 2.0 ms).

Low-speed air inflow (10 m/s)

The reactive flow is ignited at 30.8 ms, with an ignition duration of 8.0 ms, concluding at 38.8 ms. Fig. 13 illustrates the initial evolution of the hydrogen flame, beginning at 31.0 ms. The initial flame kernel generated by the spark propagates both upstream and downstream at nearly the same speeds, which is notably different from other cases. The flame that propagates upstream ultimately becomes anchored around the streamwise location of x = 0.04 m.

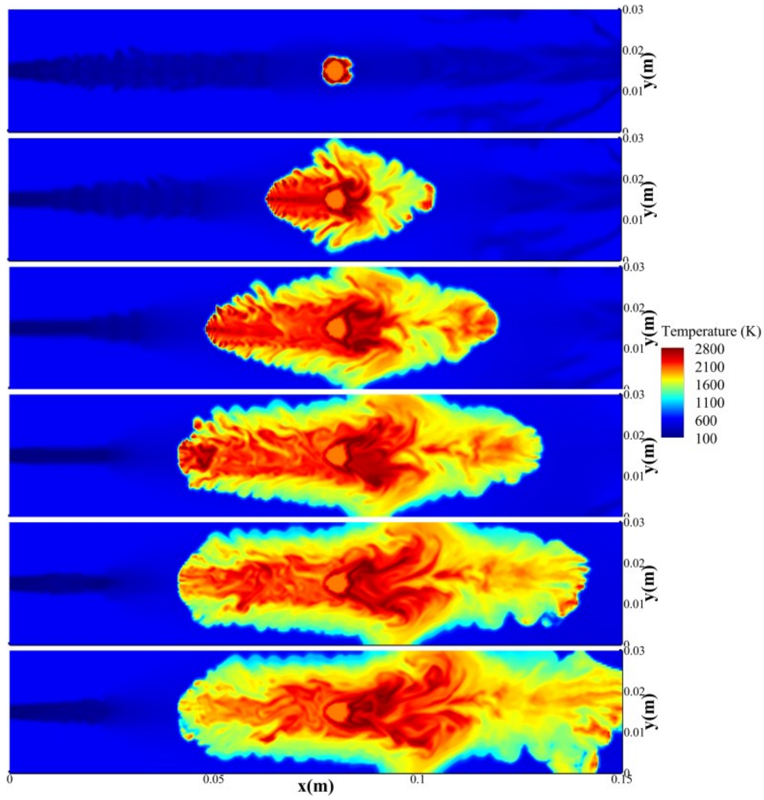

Figure 13 Flame's initial evolution of case 'Airspeed of 10 m/s for climb stage'. Time from 31.0 ms to 36.0 ms (snapshots from up to bottom taken every 1.0 ms).

The ignition spark is turned off at 38.8 ms. Fig. 14 illustrates the subsequent self-sustained propagation of the hydrogen flame. Remarkably, the flame is observed to survive within the cryogenic flow, indicating its resilience under these conditions.

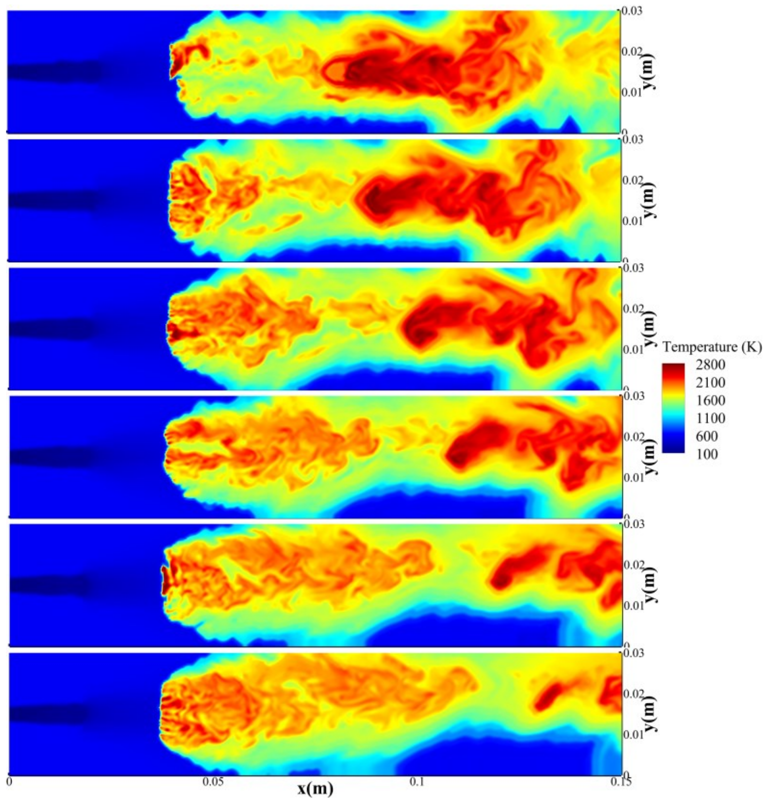

Figure 14 Flame's self-evolution of case 'Airspeed of 10 m/s for climb stage' after spark deactivation. Time from 39.0 ms to 49.0 ms (snapshots from up to bottom taken every 2.0 ms).

Cruise stage

In the cruise phase, with an inflow speed of 20 m/s, the flame could not propagate upstream and formed a stable downstream lift flame. At 10 m/s, a similar downstream propagation occurred, albeit at lower temperatures, which could reduce NOx emissions.

High-speed air inflow (20 m/s)

With an inflow air speed of 20 m/s, the reactive flow is ignited at 30.0 ms, lasting for an ignition duration of 8.0 ms until 38.0 ms. During the cruise stage, the flame kernel initiated by the spark is unable to propagate upstream. Instead, the hydrogen flame propagates rapidly downstream.

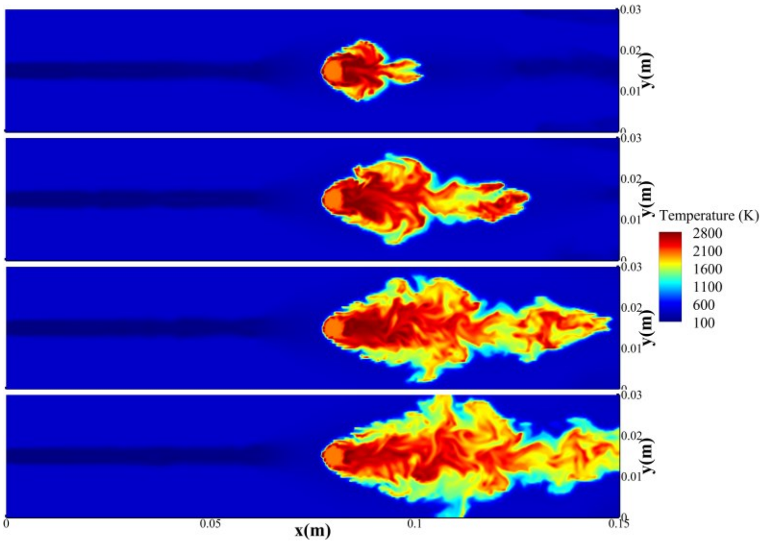

Figure 15 Flame's initial evolution of case 'Airspeed of 20 m/s for cruise stage'. Time from 31.0 ms to 34.0 ms (snapshots from up to bottom taken every 1.0 ms).

At 38.0 ms, the spark is turned off. It is observed that the hydrogen flame can be sustained downstream of the spark's position, ultimately leading to the establishment of a turbulent lift flame, as shown in Fig. 16.

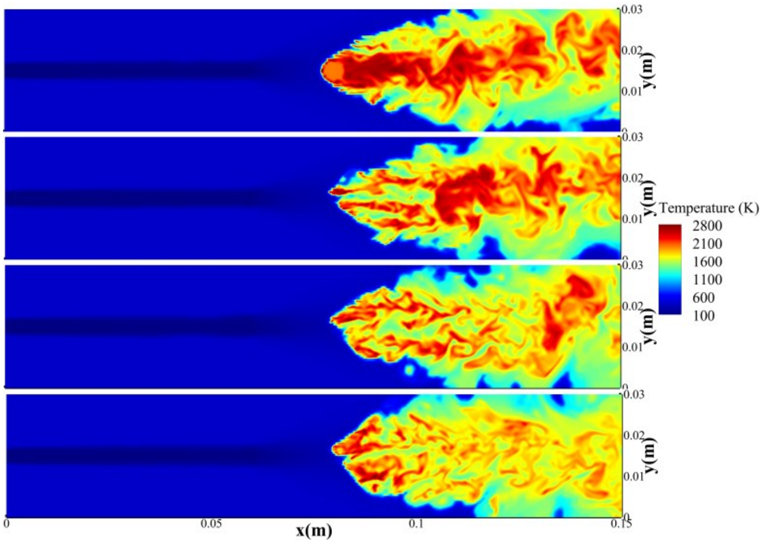

Figure 16 Flame's self-evolution of case 'Airspeed of 20 m/s for cruise stage' after spark deactivation. Time from 38.0 ms to 44.0 ms (snapshots from up to bottom taken every 2.0 ms).

Low-speed air inflow (10 m/s)

With an inflow air speed of 10 m/s, the reactive flow is ignited at 30.0 ms, with an ignition duration of 8.0 ms until 38.0 ms. As depicted in Fig. 17, the flame propagates more slowly downstream from the ignition point due to the lower inflow speed. Similar to the case with an inflow speed of 20 m/s during the cruise stage, the flame does not propagate upstream.

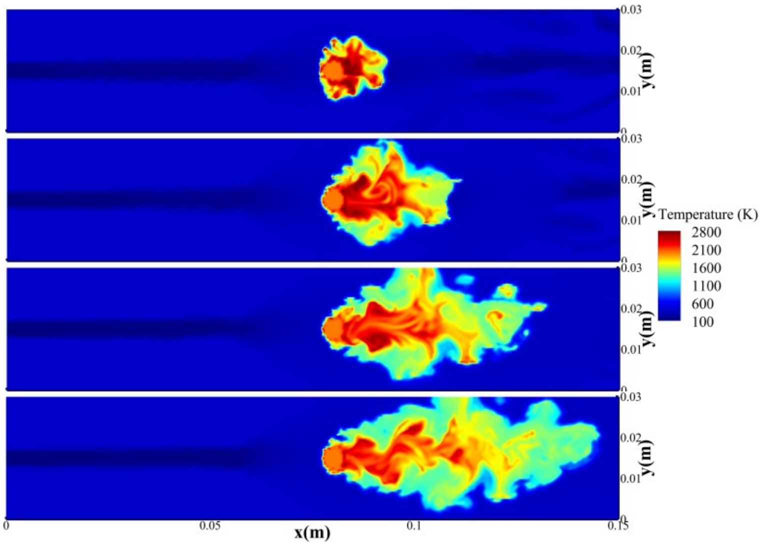

Figure 17 Flame's initial evolution of case 'Airspeed of 10 m/s for cruise stage'. Time from 31.0 ms to 37.0 ms (snapshots from up to bottom taken every 2.0 ms).

After the spark is turned off, the hydrogen flame can survive in the cryogenic flow, as shown in Fig. 18. It is observed that the flame exhibits a significantly lower temperature compared to other cases, which is advantageous for reducing NOx production.

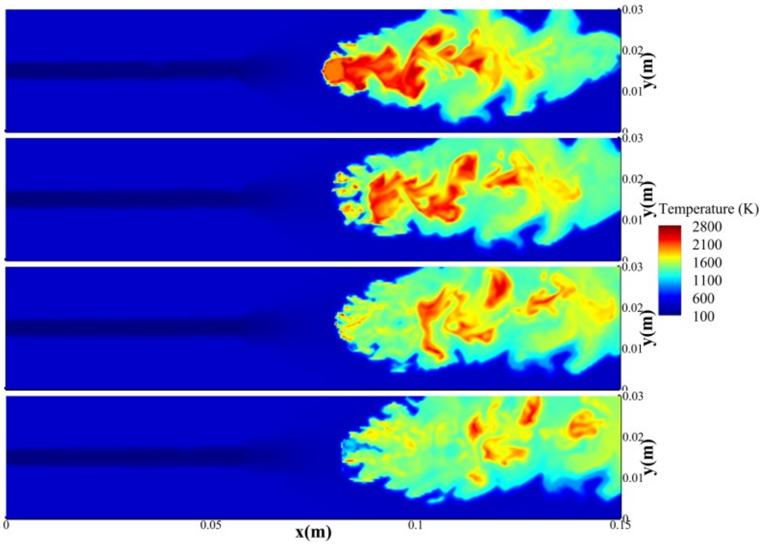

Figure 18 Flame's self-evolution of case 'Airspeed of 10 m/s for cruise stage' after spark deactivation. Time from 38.0 ms to 44.0 ms (snapshots from up to bottom taken every 2.0 ms).

Descent/Landing stage

For descent at 10 m/s, the flame propagated only downstream, exhibiting local quenching due to reduced inflow pressure. For the 20 m/s, the flame is not stable after spark deactivation.

High-speed air inflow (20 m/s)

As the inflow air has a relatively high speed of 20 m/s, the reactive flow is ignited from 14 ms and last 8 ms. The evolution of the flame is described in Fig. 19 by using the temperature distributions at different times.

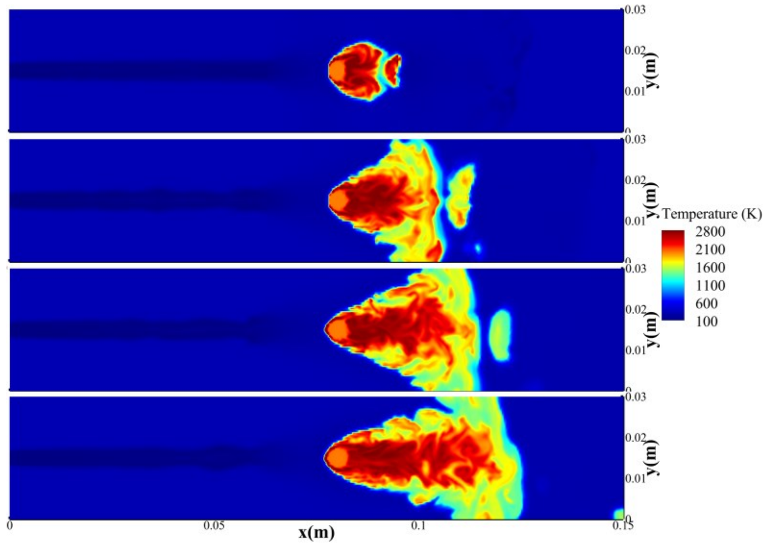

Figure 19 Flame's initial evolution of case 'Airspeed of 20 m/s for descent/landing stage'. Time from 15.0 ms to 21.0 ms (snapshots from up to bottom taken every 2.0 ms).

After the spark is turned off, the flame can be stabilised in the combustion chamber, as shown in Fig. 20. The flame is anchored in the chamber.

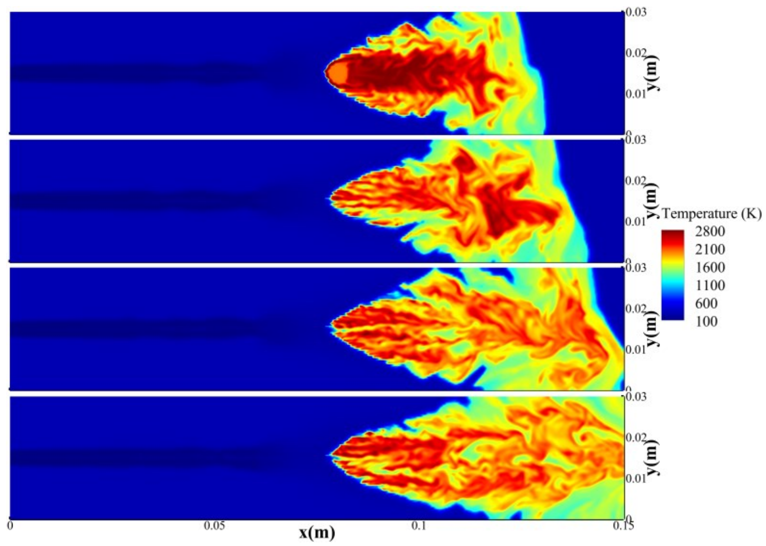

Figure 20 Flame's self-evolution of case 'Airspeed of 20 m/s for descent/landing stage' after spark deactivation. Time from 22.0 ms to 28.0 ms (snapshots from up to bottom taken every 2.0 ms).

Low-speed air inflow (10 m/s)

With an inflow air speed of 10 m/s, the reactive flow is ignited at 30.0 ms, lasting for an ignition duration of 8.0 ms until 38.0 ms. Similar to the cruise stage with low static pressure, the flame only propagates downstream and is unable to propagate upstream, as shown in the following snapshots in Fig. 21.

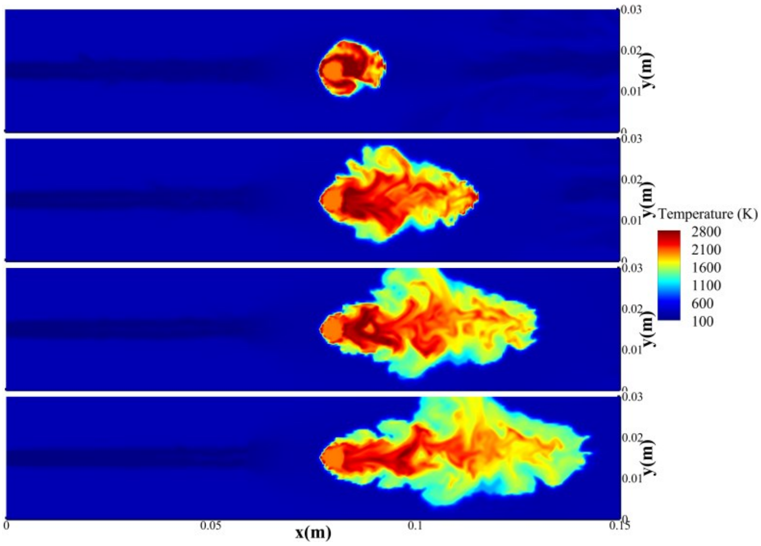

Figure 21 Flame's initial evolution of case 'Airspeed of 10 m/s for descent/landing stage'. Time from 31.0 ms to 37.0 ms (snapshots from up to bottom taken every 2.0 ms).

After the spark is turned off, it is observed that the overall flame can still be sustained in the flow, as shown in Fig. 22. However, combustion stability is compromised, leading to localised quenching events.

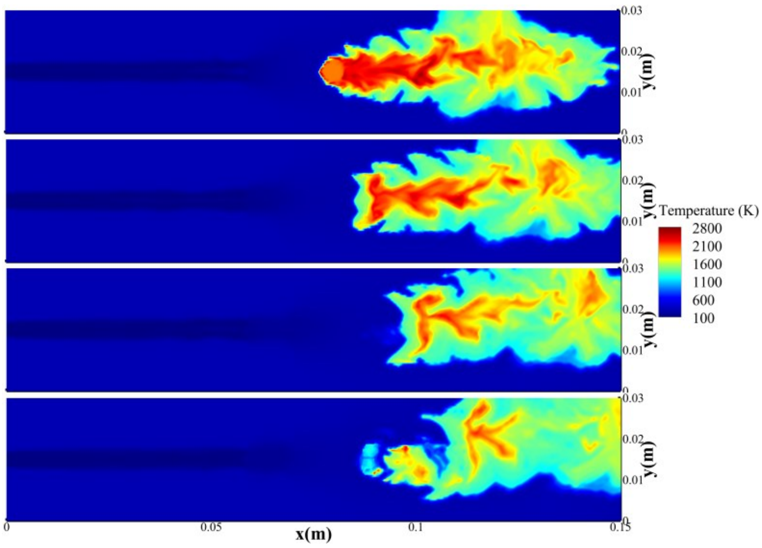

Figure 22 Flame's self-evolution of case 'Airspeed of 10 m/s for descent/landing stage' after spark deactivation. Time from 38.0 ms to 44.0 ms (snapshots from up to bottom taken every 2.0 ms).

Hydrogen combustion in off-design flight scenarios

Take-off under "hot and high" conditions

Airports at high altitudes and hot climates impose challenging conditions for engine operations due to lower ambient pressures and higher temperatures. This scenario tested cryogenic hydrogen combustion under such off-design conditions. The combustion chamber inlet parameters were set to simulate a high-altitude (2,000-3,000 metres) and high-temperature (30-40°C) environment, with air inflow speeds of 10 m/s and 20 m/s.

High-speed air inflow (20 m/s)

Ignition occurred between 15 ms and 23 ms. As shown in Fig. 23, the flame propagated rapidly towards the inlet after spark activation. The flame eventually anchored near the inlet, enveloping the core jet of cold hydrogen.

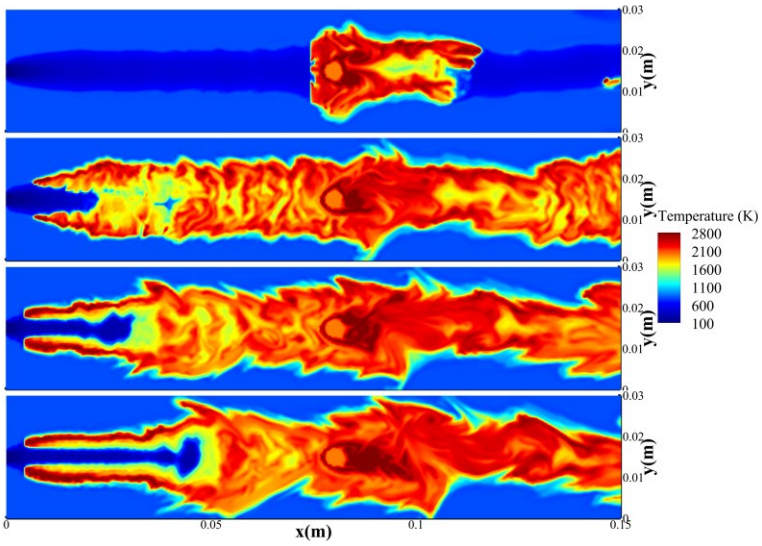

Figure 23 Flame's initial evolution of case 'Airspeed of 20 m/s for take-off under hot and high conditions'. Time from 16.0 ms to 19.0 ms (snapshots from up to bottom taken every 1.0 ms).

After spark deactivation at 23 ms, the flame sustained itself in the combustion chamber. As illustrated in Fig. 24, the flame topology formed an enveloping structure, ensuring safe combustion without flashback due to the non-premixed injection pattern.

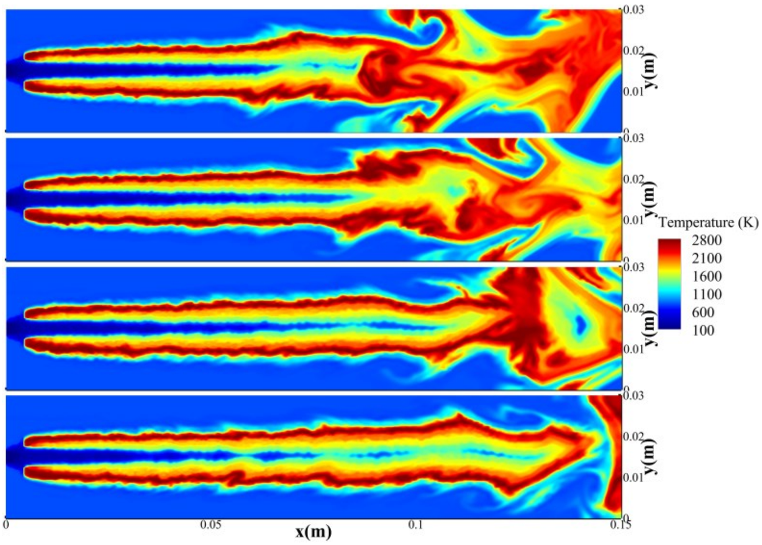

Figure 24 Flame's self-evolution of case 'Airspeed of 20 m/s for take-off under hot and high conditions' after spark deactivation. Time from 24.0 ms to 30.0 ms (snapshots from up to bottom taken every 2.0 ms).

Low-speed air inflow (10 m/s)

With ignition from 20 ms to 28 ms, the flame propagation was fast towards the inlet, similar to the high-speed case. Fig. 25 shows the flame's rapid development.

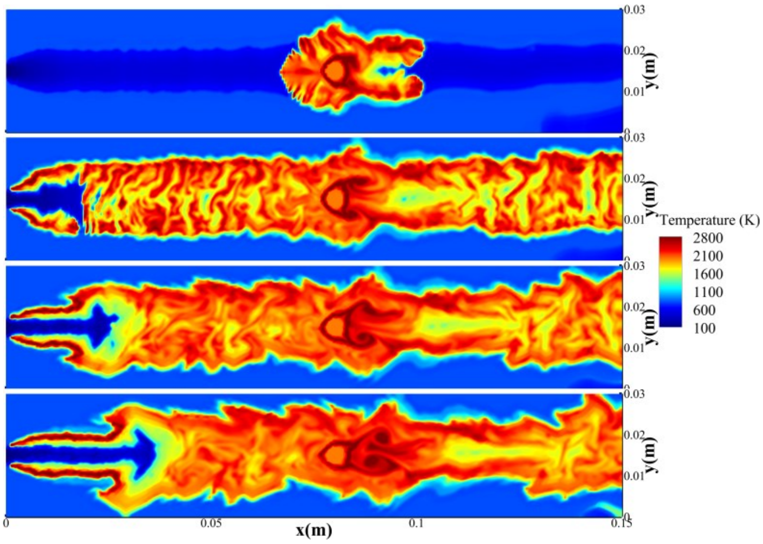

Figure 25 Flame's initial evolution of case 'Airspeed of 10 m/s for take-off under hot and high conditions'. Time from 21.0 ms to 24.0 ms (snapshots from up to bottom taken every 1.0 ms).

After the spark was deactivated, the flame established a stable, self-sustained state, forming an enveloped flame structure (Fig. 26).

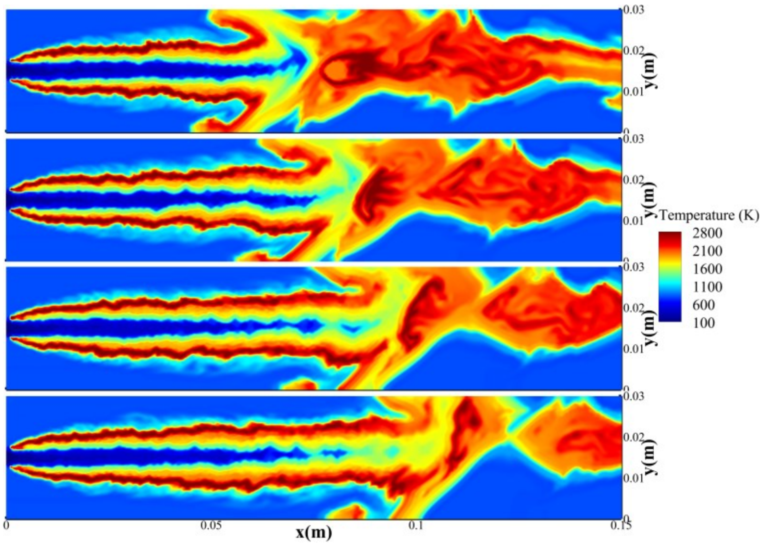

Figure 26 Flame's self-evolution of case 'Airspeed of 10 m/s for take-off under hot and high conditions' after spark deactivation. Time from 28.0 ms to 34.0 ms (snapshots from up to bottom taken every 2.0 ms).

The 'hot and high' take-off case poses a risk of flame attachment to the fuel nozzle, mainly due to the high flame speed of hydrogen fuel. Numerical tests show that the flame lift-off distance remains a few mm from the nozzle, indicating a narrow safety margin. Further combustor design considerations for hydrogen, such as injector cooling and flame holder modifications, may be needed for real-engineering implementation.

Flame out to 25,000 ft (5% max N2 shaft speed)

During engine flame-out at 25,000 ft, the windmilling state provides a low air inlet pressure and temperature, modelled at 5% max N2 shaft speed.

High-speed air inflow (20 m/s)

Ignition was initiated at 14 ms and then persisted for 8 ms. Fig. 27 shows the flame's initial development, which remained narrow due to the low pressure and temperature during the windmilling process. After spark deactivation, the flame was extinguished rapidly (Fig. 28).

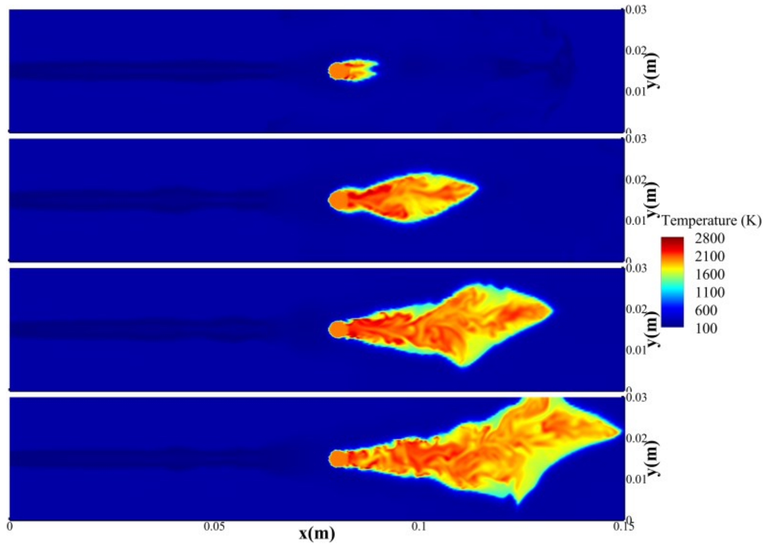

Figure 27 Flame's initial evolution of case 'Airspeed of 20 m/s for flame out to 25,000 ft with 5% max N2 shaft speed'. Time from 15.0 ms to 21.0 ms (snapshots from up to bottom taken every 2.0 ms).

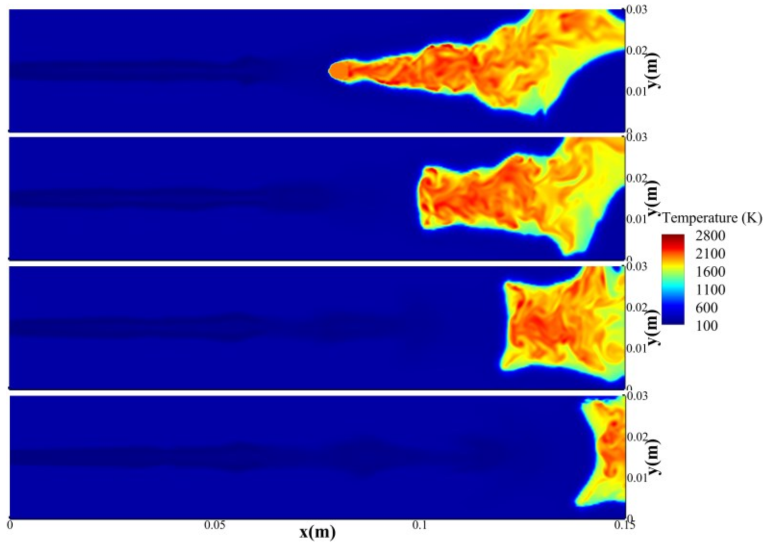

Figure 28 Flame's self-evolution of case 'Airspeed of 20 m/s for flame out to 25,000 ft with 5% max N2 shaft speed' after spark deactivation. Time from 22.0 ms to 28.0 ms (snapshots from up to bottom taken every 2.0 ms).

Low-speed air inflow (10m/s)

The flame developed slowly under a low-speed inflow of 10 m/s. Ignition was active from 30 ms to 38 ms (Fig. 29). Following spark deactivation, the flame extinguished quickly due to insufficient combustion conditions (Fig. 30).

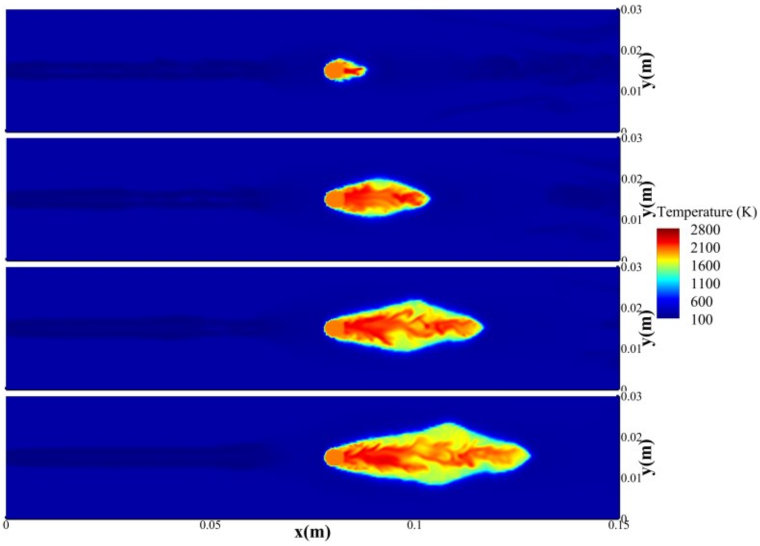

Figure 29 Flame's initial evolution of case 'Airspeed of 10 m/s for flame out to 25,000 ft with 5% max N2 shaft speed'. Time from 31.0 ms to 37.0 ms (snapshots from up to bottom taken every 2.0 ms).

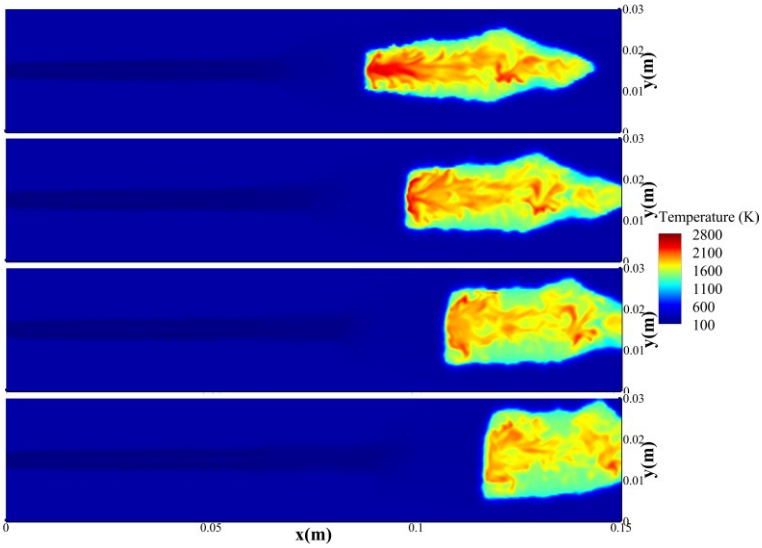

Figure 30 Flame's self-evolution of case 'Airspeed of 10 m/s for flame out to 25,000 ft with 5% max N2 shaft speed' after spark deactivation. Time from 40.0 ms to 46.0 ms (snapshots from up to bottom taken every 2.0 ms).

Flame out to 25,000 ft (20% max N2 shaft speed)

From the previous tests, we found that the flame cannot be established under the 5% max N2 shaft speed and the associated low pressure and temperature of air at the combustor inlet. This scenario increased the N2 shaft speed to 20%, yielding higher pressure and temperature for combustion.

High-speed air inflow (20 m/s)

Ignition occurred between 14 ms and 22 ms. The flame topology showed minimal differences from the 5% N2 shaft speed case (Fig. 31). After spark deactivation, the hydrogen flame was extinguished (Fig. 32).

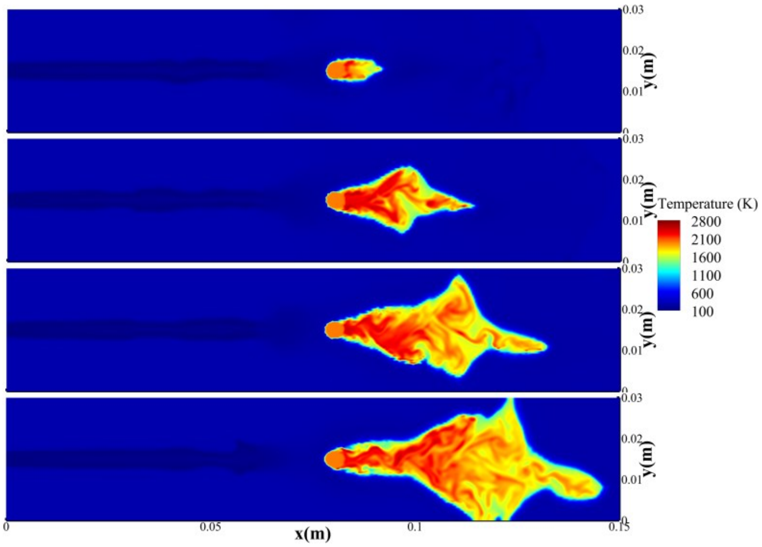

Figure 31 Flame's initial evolution of case 'Airspeed of 20 m/s for flame out to 25,000 ft with 20% max N2 shaft speed'. Time from 15.0 ms to 21.0 ms (snapshots from up to bottom taken every 2.0 ms).

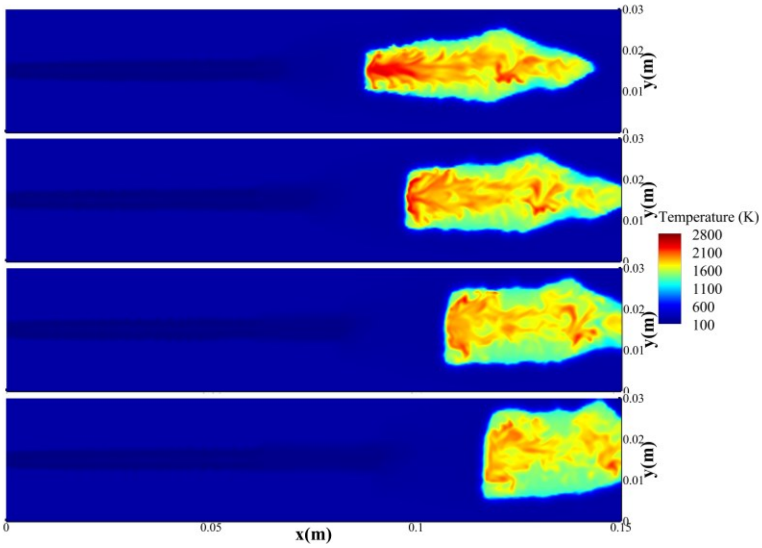

Figure 32 Flame's self-evolution of case 'Airspeed of 20 m/s for flame out to 25,000 ft with 20% max N2 shaft speed' after spark deactivation. Time from 22.0 ms to 28.0 ms (snapshots from up to bottom taken every 2.0 ms).

Low-speed air inflow (10 m/s)

For a low-speed airflow, ignition persisted from 30 ms to 38 ms. The flame developed slowly from the ignition kernel (Fig. 33). Despite initial flame propagation, the flame was extinguished after spark deactivation (Fig. 34).

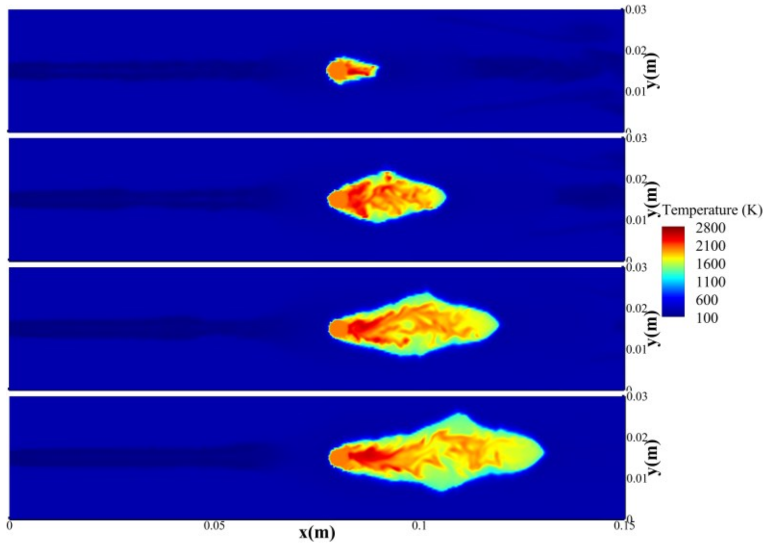

Figure 33 Flame's initial evolution of case 'Airspeed of 10 m/s for flame out to 25,000 ft with 20% max N2 shaft speed'. Time from 31.0 ms to 37.0 ms (snapshots from up to bottom taken every 2.0 ms).

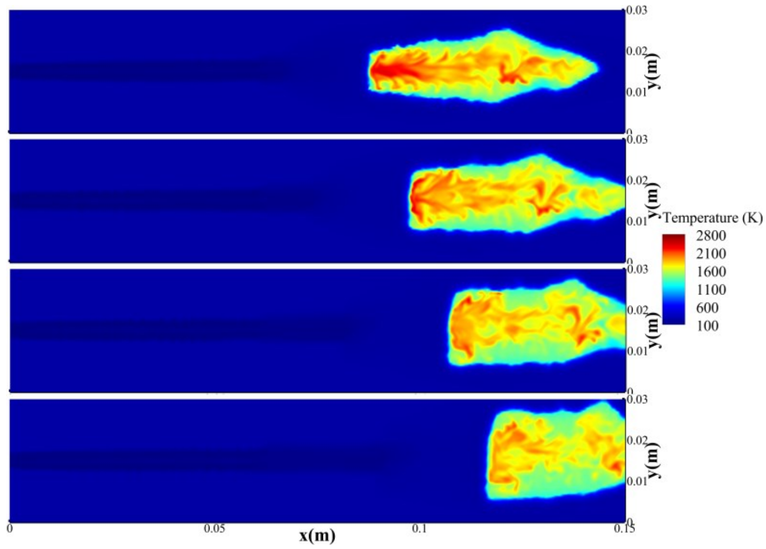

Figure 34 Flame's self-evolution of case 'Airspeed of 10 m/s for flame out to 25,000 ft with 20% max N2 shaft speed' after spark deactivation. Time from 40.0 ms to 46.0 ms (snapshots from up to bottom taken every 2.0 ms).

Relight during cruise (20% max N2 shaft speed)

This off-design test examined the possibility of relighting during a cruise at 37,000 ft under windmilling conditions with 20% max N2 shaft speed.

High-speed air inflow (20 m/s)

Ignition commenced at 11 ms and lasted for 8 ms. As shown in Fig. 35, the combustion area was narrow, and local quenching occurred due to low pressure. The flame extinguished quickly after spark deactivation (Fig. 36).

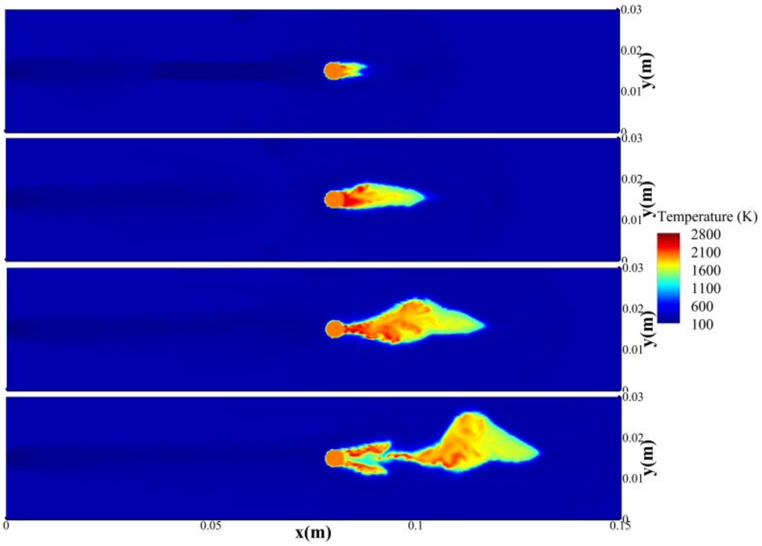

Figure 35 Flame's initial evolution of case 'Airspeed of 20 m/s for Relight during cruise'. Time from 12.0 ms to 18.0 ms (snapshots from up to bottom taken every 2.0 ms).

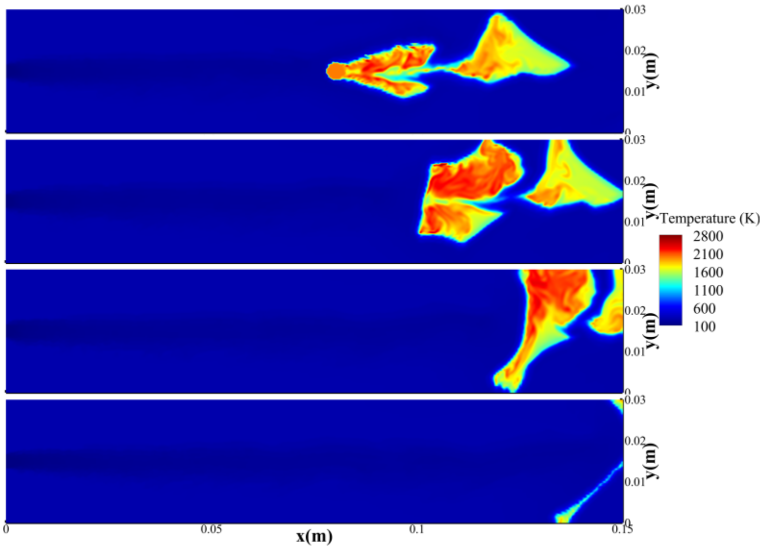

Figure 36 Flame's self-evolution of case 'Airspeed of 20 m/s for Relight during cruise' after spark deactivation. Time from 19.0 ms to 25.0 ms (snapshots from up to bottom taken every 2.0 ms).

Low-speed air inflow (10 m/s)

Under low-speed inflow, ignition started at 30 ms and persisted until 38 ms. The flame developed more stably compared to the high-speed case (Fig. 37). However, after spark deactivation, the flame was extinguished, likely due to slow chemical reaction rates at low pressures (Fig. 38).

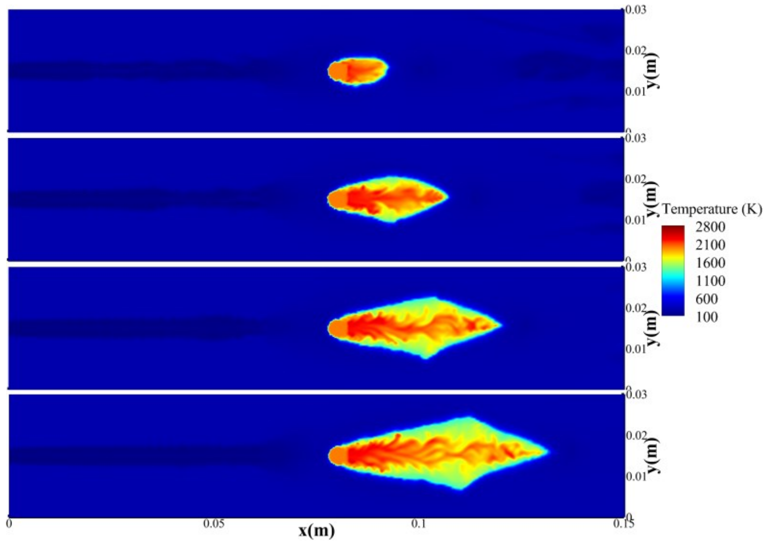

Figure 37 Flame's initial evolution of case 'Airspeed of 10 m/s for Relight during cruise'. Time from 32.0 ms to 38.0 ms (snapshots from up to bottom taken every 2.0 ms).

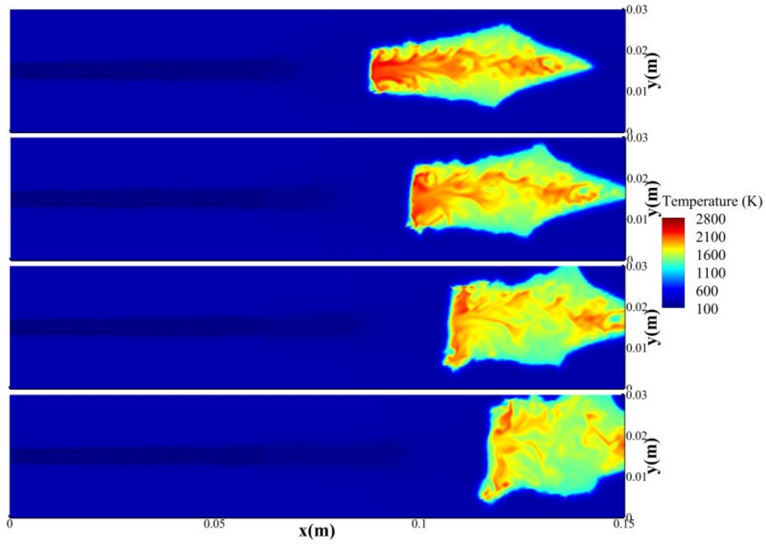

Figure 38 Flame's self-evolution of case 'Airspeed of 10 m/s for Relight during cruise' after spark deactivation. Time from 40.0 ms to 46.0 ms (snapshots from up to bottom taken every 2.0 ms).

Hydrogen combustion during flight state transitions

In this section, we will investigate the hydrogen combustion behaviours under the flight state transitions, including the transition from take-off to climb, the transition from climb to cruise, and the transition from cruise to descent/landing. Special arrangements for the set up are as follows,

- Since the pressure and temperature of the combustion chamber inlet are changed during the flight state transition, the variation is a linear changing process instead of an abrupt transition to mimic the real situation in which pilots adjust engine power settings gradually during flight phase transitions.

- The inlet mass flow rate of cryogenic hydrogen is varied accordingly to keep the equivalence ratio equalling unity. We set up the transition time of 10 ms for each test to see whether the flame can be stabilised during the short time period. If the answer is yes, the hydrogen can be expected to be stable for a longer transition period. The combustion is continuously operated, and the spark ignition is not used during the test.

Transition from take-off to climb

High-speed air inflow (20 m/s)

Fig. 39 displays the hydrogen flames during the transition process from take-off to climb. The static pressure of inflow air decreases from 8 bar towards 6 bar and the static temperature decreases from 700 K to 600 K. It is found that the hydrogen combustion is stable during this transition process.

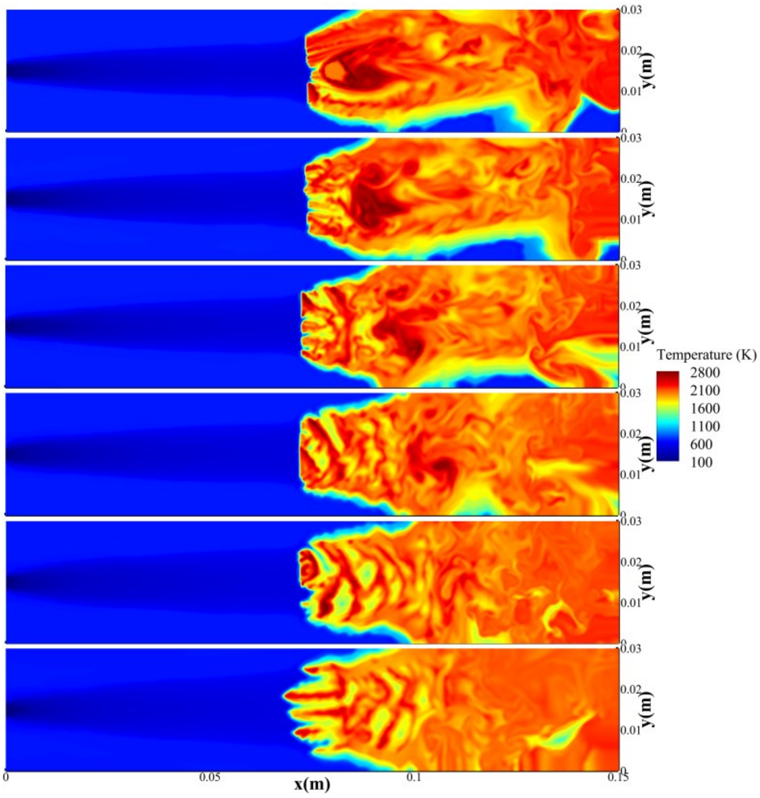

Figure 39 Flame's self-evolution of case 'Airspeed of 20 m/s for the transition from take-off to climb' (snapshots from up to bottom taken every 1.0 ms).

Low-speed air inflow (10 m/s)

For the low-speed inflow, the hydrogen is also stable during the transition process. As the inlet pressure and inlet temperature decrease from the take-off to climb stages, it is found that the temperature distribution becomes uniform, as shown in Fig. 40.

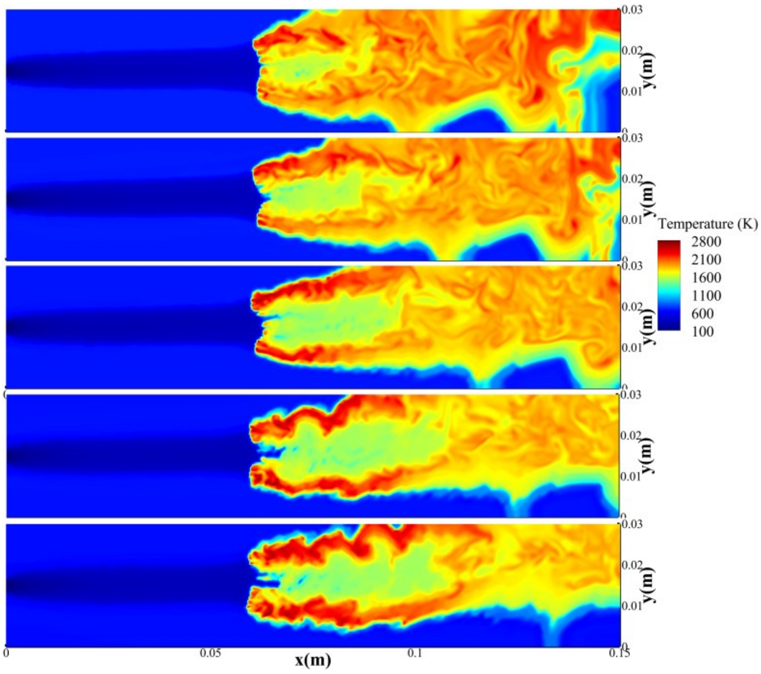

Figure 40 Flame's self-evolution of case 'Airspeed of 10 m/s for the transition from take-off to climb' (snapshots from up to bottom taken every 2.0 ms).

Transition from climb to cruise

Both the pressure and temperature of the combustion chamber inlet drop during the transition from climb to cruise. At the combustion air inlet, the static pressure decreases from 6 bar to 2 bar and the static temperature decreases from 600 K to 400 K.

High-speed air inflow (20 m/s)

Fig. 41 shows the development of the hydrogen flame topology during the flight transition from climb to cruise. The tip of the flame is found to change from a 'flat' tip to a 'pointed' one. The temperature distribution in the combustion chamber becomes more non-uniform.

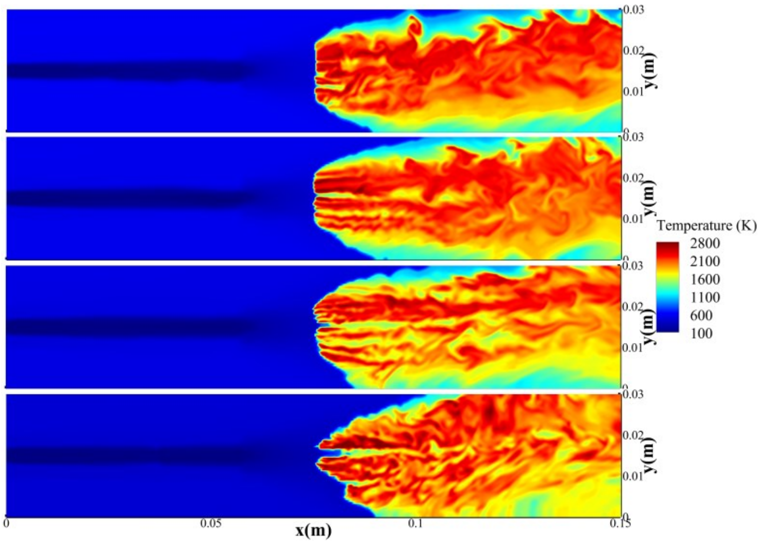

Figure 41 Flame's self-evolution of case 'Airspeed of 20 m/s for the transition from climb to cruise' (snapshots from up to bottom taken every 3.0 ms).

Low-speed air inflow (10 m/s)

Fig. 42 shows the flame evolution as the speed of air inflow is slow. Generally, the hydrogen flame is stable during the transition stage.

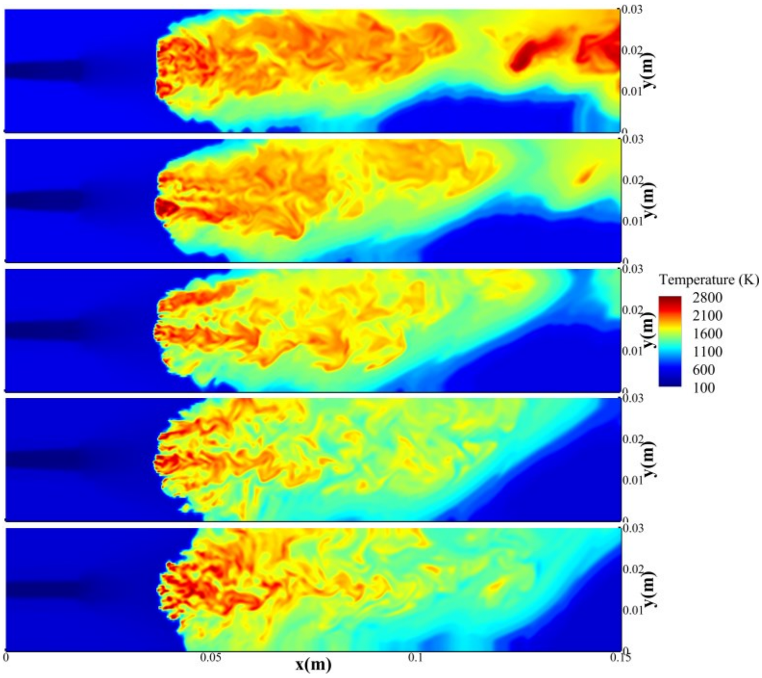

Figure 42 Flame's self-evolution of case 'Airspeed of 10 m/s for the transition from climb to cruise' (snapshots from up to bottom taken every 3.0 ms).

Transition from cruise to descent/landing

During the flight stages transited from cruise to descent/landing, the static pressure at the combustion chamber inlet increases from 2 bar to 3 bar and the static temperature decreases from 400 K to 300 K. Compared to the other two transition stages, the transition from cruise to descent/landing does not have huge change of pressures and temperatures at the chamber inlet, and therefore the hydrogen flame topology/structure and the combustion field do not have obvious change.

High-speed air inflow (20 m/s)

As the air inflow at the combustion chamber inlet is 20 m/s, the flame evolution during the transition process is shown in Fig. 43. The hydrogen combustion is table. Flame topology and the combustion field seem do not to have obvious change.

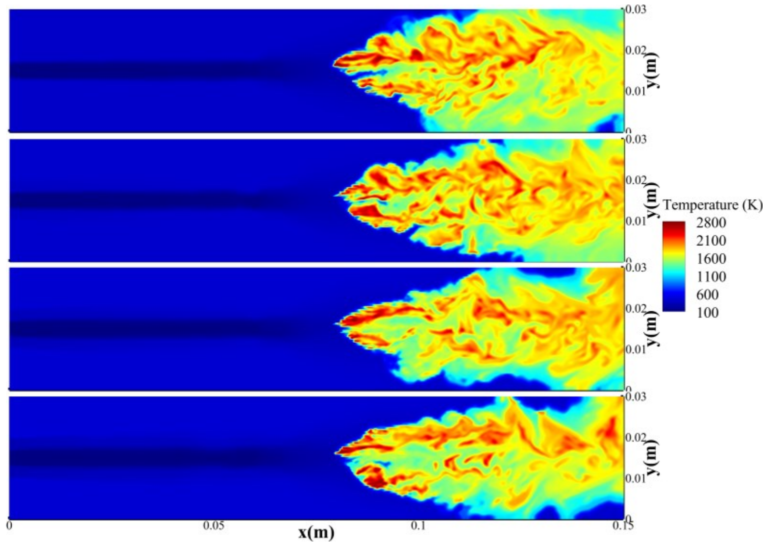

Figure 43 Flame's self-evolution of case 'Airspeed of 20 m/s for the transition from cruise to descent/landing' (snapshots from up to bottom taken every 3.0 ms).

Low-speed air inflow (10 m/s)

As the inflow of air at the combustion chamber inlet is decreased to 10 m/s, the hydrogen flame is found to be stabilised during the transition process, as shown in Fig. 44.

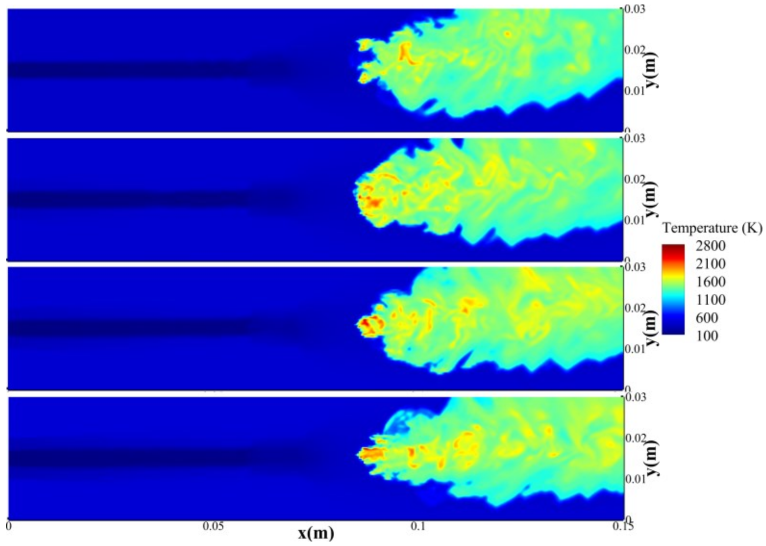

Figure 44 Flame's self-evolution of case 'Airspeed of 20 m/s for the transition from cruise to descent/landing' (snapshots from up to bottom taken every 3.0 ms).

Chapter 6

Summary and Outlook

Summary

Table 3 summarises the hydrogen combustion characteristics observed across all numerical tests in this study. The results confirm that cryogenic hydrogen combustion remains stable under steady flight conditions, from take-off to landing, as well as during flight phase transitions when the combustion chamber inlet airflow is adjusted.

For off-design scenarios, a potential risk of flame attachment to the fuel injection nozzle was identified, necessitating the development of design strategies to mitigate this issue. Additionally, during relight tests, hydrogen flames were extinguished after spark deactivation, highlighting the need for alternative ignition strategies such as extended ignition duration to ensure successful relight.

Table 3 Summary of hydrogen combustion tests.

H2 Combustion in Steady Flight Conditions	Stable Combustion?	Solution
Take off (Air inlet: 8 bar, 700 K)	Yes	N/A
	Yes	N/A
Climb (Air inlet: 6 bar, 600 K)	Yes	N/A
	Yes	N/A
Cruise (Air inlet: 2 bar, 400 K)	Yes	N/A
	Yes	N/A

H2 Combustion in Steady Flight Conditions	Stable Combustion?	Solution
Desent/Landing (Air inlet: 3 bar, 300K)	Yes Yes	N/A N/A

H2 Combustion in Off-Design Flight Scenarios	Stable Combustion?	Solution
Take-off under “hot and high” (Air inlet: 7 bar, 800 K)	Yes Yes	N/A N/A
Flame out to 25,000 ft (5% max N2 shaft speed) (Air inlet: 0.44 bar, 250 K)	No No	Increase ignition duration Increase ignition duration
Flame out to 25,000 ft (20% max N2 shaft speed) (Air inlet: 0.57 bar, 280K)	No No	Increase ignition duration Increase ignition duration
Relight at 37,000 ft	No	Increase ignition duration

H2 Combustion in Off-Design Flight Scenarios	Stable Combustion?	Solution
(20% max N2 shaft speed) (Air inlet: 0.39 bar, 280K)	No	Increase ignition duration
Continuous ignition during take-off stage (Air inlet: 8 bar, 700K)	Yes Yes	N/A N/A

H2 Combustion During Flight State Transitions	Stable Combustion?	Solution
From Take off (Air inlet: 8 bar, 700 K) to Climb (Air inlet: 6 bar, 600 K)	Yes Yes	N/A N/A
From Climb (Air inlet: 6 bar, 600 K) to Cruise: (Air inlet: 2 bar, 400 K)	Yes Yes	N/A N/A

H2 Combustion During Flight State Transitions	Stable Combustion?	Solution
From Cruise (Air inlet: 2 bar, 400 K) to Desent/Landing (Air inlet: 3 bar, 300 K)	Yes	N/A
	Yes	N/A

Utilising hydrogen at cryogenic temperature (80 K) for combustion offers several advantages, including higher fuel density, improved cooling, reduced flashback risks, and enhanced injection momentum. The research suggests the potential viability of cryogenic hydrogen combustion across various flight stages. The simulations demonstrated a safely anchored and stable single-jet hydrogen flame, providing fundamental insights into flame anchoring, lift-off distances, and temperature distributions. However, to establish feasibility for full-scale gas turbine applications, further research is required to evaluate multi-nozzle configurations and flame interactions in realistic combustor conditions.

- Flame temperature.
  - Highest flame temperatures occur during take-off, climb, take-off to climb transition, and hot and high take-off conditions.
  - Stable combustion is maintained at reduced flame temperatures during cruise and landing stages.
- Lift-off distance.
  - Across all flight stages, the flames maintain a lift-off distance, ensuring safe separation between the hot flame and the fuel nozzle, even under worst-case scenarios like hot and high take-off, reducing flashback risks.
- Air inflow speed and flame behaviour.
  - Flame length & anchor points across flight phases. For take-off, climb, and transitions (higher pressure & temperature), lower airflow speed (10 m/s) leads to a shorter flame, anchored upstream, closer to fuel injection. Higher speed (20 m/s) leads to a longer flame, anchored further downstream. For cruise, descent/landing, and transitions (lower pressure & temperature), lower speed (10 m/s) results in a slightly longer flame, anchored downstream. Higher speed (20 m/s) has a slightly shorter flame, anchored upstream.

    - Implications on combustor design. For the optimised airflow management, a shorter flame reduces thermal stress and ensures efficient combustion but can bring a risk of flash back. A longer flame may cause non-uniform temperature distribution uniformity, affecting turbine performance. For adaptive fuel injection strategies, the combustor should regulate air distribution to maintain a stable flame anchor throughout flight. Variable injector designs can control flame position and temperature uniformity across different operating conditions.
    - Slower airflow (10 m/s) contributes to reduced flame temperatures and reducing NOx emissions. However, lower airspeeds may also result in higher total pressure losses during air deceleration, requiring careful diffuser design.
- Relight stability.
    - Flame propagation is slow during relight after flame-out and extinguishes after spark deactivation.
    - Increasing ignition duration is recommended to ensure the generation of sufficient hot combustion products for sustained combustion.

Flame length and anchoring vary with airflow speed and flight phase, influencing combustion performance. Future combustor designs should optimise air-fuel mixing to ensure efficiency, durability, and emissions control in hydrogen gas turbines across all flight phases.

Future research

Future research will focus on the following areas to address the limitations of this study and extend the understanding of cryogenic hydrogen combustion in a realistic multi-nozzle gas turbine combustor:

- Multi-Nozzle combustion and flame stabilization:
    - Investigate parallel-flow multi-nozzle configurations to analyse interactions between multiple cryogenic hydrogen jets and develop a comprehensive combustor design.
    - Explore vortex-stabilised hydrogen flames, assessing how swirl-stabilisation can improve flame anchoring and overall combustion stability in multi-nozzle systems.
    - Optimise jet spacing and injection strategies to balance mixing efficiency and flame stability, minimizing flashback risks and pressure losses in multi-nozzle (micro-mixing) configurations.

    - Develop and validate a digital twin model for multi-nozzle cryogenic hydrogen combustion, incorporating experimental data to improve predictive accuracy.
- Hydrogen safety and injector system reliability.
    - Analyse full-bore hydrogen injector nozzle failures to assess the potential hazards, pressure fluctuations, and combustion instability that could arise in an operational gas turbine.
    - Evaluate potential thermal management strategies to prevent fuel overheating and phase change issues.
    - Establish safe ignition conditions for “hot and high” take-off scenarios, ensuring stable combustion without flame attachment to the injection nozzle.
- In-flight relight operation.
    - Establish conditions for successful in-flight relight, optimizing ignition strategies, ignition duration, and fuel staging to achieve reliable relight at high altitudes and low pressures.
    - Investigate high-altitude ignition challenges, including flame quenching and ignition delay, to improve combustor design for hydrogen-powered aviation applications.

APPENDIX A

References

[1] Ren Z. CFD of H2 flame. 1st Hydrogen combustion workshop, Loughborough University, Loughborough, United Kingdom, 29 June, 2022.

[2] Poling B E, Prausnitz J M, O'connell J P. The properties of gases and liquids[M]. New York: Mcgraw-hill, 2001.

[3] Boivin P, Cannac M A, Le Métayer O. A thermodynamic closure for the simulation of multiphase reactive flows[J]. International Journal of Thermal Sciences, 2019, 137: 640-649.

[4] Burcat A, Ruscic B. Third millenium ideal gas and condensed phase thermochemical database for combustion (with update from active thermochemical tables)[R]. Argonne National Lab.(ANL), Argonne, IL (United States), 2005.

[5] Linstrom P J, Mallard W G. The NIST Chemistry WebBook: A chemical data resource on the internet[J]. Journal of Chemical & Engineering Data, 2001, 46(5): 1059-1063.

[6] Li J, Zhao Z, Kazakov A, et al. An updated comprehensive kinetic model of hydrogen combustion[J]. International journal of chemical kinetics, 2004, 36(10): 566-575.

[7] Hu X Y, Wang Q, Adams N A. An adaptive central-upwind weighted essentially non-oscillatory scheme[J]. Journal of Computational Physics, 2010, 229(23): 8952-8965.

[8] Ren Z, Giannissi S, Venetsanos A G, et al. International Journal of Hydrogen Energy, 2022, 47(67): 29184-29194.

[9] A. Friedrich, A. Veser, N. Kotchourko, M. Kuznetsov, T. Jordan, High-pressure cryogenic hydrogen releases (unignited DISCHA), PRESLHY Dissemination Conference, 5-6 May, 2021.

[10] Simoneau R J, Hendricks R C. Two-phase choked flow of cryogenic fluids in converging-diverging nozzles[R]. NASA Technical Reports 1484, 1979.

[11] Kuznetsov M, Denkevits A, Veser A, et al. Flame propagation regimes and critical conditions for flame acceleration and detonation transition for hydrogen-air mixtures at cryogenic temperatures[J]. International Journal of Hydrogen Energy, 2022, 47(71): 30743-30756.

[12] Brend M. H2: Absolute zero-carbon propulsion systems. 1st Hydrogen combustion workshop, Loughborough University, Loughborough, United Kingdom, 29 June, 2022.

[13] Clarke J., et al. Cryogenic hydrogen jet and flame for clean energy applications: progress and challenges. Energies, 2023: 16.11: 4411.

APPENDIX B

Simulation Results and Certification Requirements

Background to Simulations

Simulation studies centred on the combustion of a single jet of cryo-compressed hydrogen at a temperature of 80K (-193°C) injected parallel to the combustion chamber air flow. Shearing of the hydrogen jet with the air flow ensured fuel air/mixing. Hydrogen flame speed is an order of magnitude greater than kerosene. The assumption was made that the air diffuser up stream of the combustion chamber could be modified to produce higher inlet velocities to cope with the hydrogen flame speed. Typical air velocities in contemporary gas turbines are around 5ms^{-1}. The simulation assumed discreet valves of 10 and 20 ms^{-1}.

The simulation results come with a caveat. Simulation of the ignition and combustion of a single hydrogen flame is not equivalent to the simulation of hydrogen combustion in a complicated co-axial gas turbine under FADEC (Full Authority Digital Engine Control) control. However, the results do high-light possible certification challenges.

Scenarios at Aircraft Level

The aircraft scenario is a single aisle airliner equipped with a “CFM-56” type engine that combusts hydrogen. Justification is that once hydrogen electric CS 23 aircraft are certified and in-service the next step could be hydrogen fuelled single aisle aeroplanes. Operational conditions (take-off, climb, cruise, descent, landing and in-flight relight) would be similar to the CFM 56 currently powering the Airbus A320.

Scenarios at Engine Level

The engine scenario assumption is that of a “CFM 56” type that has been modified by replacing fuel injectors with those suitable for cryo-compressed hydrogen and combustion chamber air velocities increased for the higher hydrogen flame speed.

ICAO Annex 16: Environmental Protection Volume II – Aircraft Engine Emissions

The Committee on Aviation Environmental Protection (CAEP) working group 3 is assessing *ICAO Annex 16: Environmental Protection Volume II – Aircraft Engine Emissions* with respect to NOx emissions. The emissions in the vicinity of airports from modern engines will be considered and the possibility of extending engine emission NOx limits for full flight conditions. NOx is generated by hot exhaust gases impinging on atmospheric air and causing a reaction between the air’s nitrogen and oxygen. The simulation results showed the highest flame temperatures occur during take-off, climb, the transition from take-off to climb, and take-off under 'hot and high' scenarios. Compliance with the current ICAO NOx standards be required for a future hydrogen combusting engine certification. The simulations show high combustion temperatures at take-off and climb (i.e. in the vicinity of the airport), inferring higher NOx emissions. The simulations showed cooler flame temperatures during cruise and climb, inferring lower NOx emissions. CAEP Working Group 3 might extend NOx emission limits to full flight conditions in the future.

CS 25.105 Take-off

CS 25.105(a) requires:

"*The take-off speeds prescribed by CS 25.107, the accelerate-stop distance prescribed by CS 25.109, the take-off path prescribed by CS 25.111, the take-off distance and take-off run prescribed by CS 25.113, and the net take-off flight path prescribed by CS 25.115, must be determined in the selected configuration for take-off at each weight, **altitude, and ambient temperature** within the operational limits selected by the applicant*."

The "hot and high" scenario is for take-off at a high-altitude airport that has hot days. Usually, certification flight tests are undertaken to show compliance with the altitude and ambient temperature aspects of CS 25.105(a). Engine thermodynamic efficiency will be decreased under "hot and high" take-off conditions (warm and less dense engine inlet air). The reduced air density will also reduce aircraft lift. Reduced thrust and lift makes "hot and high" a certification test point. "Hot and high" simulation results show that after ignition the flame rapidly propagates towards the inlet nozzle, but without attaching. The challenge to certification would be to demonstrate there was no risk of attachment and flash-back through the hydrogen fuel system under "hot and high" conditions.

CS 25.903 Engines – (e) Restart Capability

CS 25.903(e) (2) states:

"An altitude and airspeed envelope must be established for in-flight engine restarting, and each engine must have a restart capability within that envelope."

Flame re-light simulations at 25,000 and 37,000ft showed rapid flame extinguishing after a simulated attempt at re-light. The simulations considered wind-milling engine high-pressure shaft speeds (N2) of 5% and 20% N2. Recall, these results are for a single hydrogen flame but suggest that the requirement to establish a certified re-light envelope for the entire engine will be challenging.

CS-E 720 Continuous Ignition

The certification requirement is to show that "*continuous ignition systems are safe and effective in the conditions for which their use is permitted or required*." Guidance on the rule gives the example of continuous ignition being necessary when taking off with the risk of water or slush engine ingestion. Simulation work has suggested continuous ignition might be required for cryo-compressed hydrogen in-flight re-light.

Operationally, the need for re-light might occur in cruise at 37,000ft. The pilot might choose to attempt a wind-milling quick relight, N2 shaft speed still being sufficiently high

(>>20%). The procedure would be to switch the engine master OFF then ON. It has to be demonstrated that this procedure consistently re-lights the engine within 30 seconds of fuel flow.

Once at 25,000ft and with stabilised wind-milling condition the FADEC can control fuel flow given current engine and environmental parameters to optimise re-light. If N2 is below 20% the FADEC will command starter engagement to increase N2.

The challenge to certification is to show that continuous ignition systems are safe and effective under these in-flight engine re-light conditions.

CS 25.981 Fuel System – General

CS 25.981(a) mentions "*Each fuel system must be constructed and arranged to ensure a flow of fuel at a rate and pressure established for proper engine functioning*." It is the responsibility of the airframer to provide a certified fuel system that ensures proper engine functioning. For an engine fuelled by cryo-compressed hydrogen 25.981(a) might also need to mention ensuring a flow of fuel in the established thermodynamic state and cryogenic temperature.